Inorganic Chemistry

Article

pubs.acs.org/IC

Controllable Formation of Heterotrimetallic Coordination Compounds: Systematically Incorporating Lanthanide and Alkali Metal Ions into the Manganese 12-Metallacrown-4 Framework

Michael R. Azar,[†] Thaddeus T. Boron, III,[⊥] Jacob C. Lutter,[†] Connor I. Daly,[†] Kelcie A. Zegalia,[†] Ruthairat Nimthong,[∥,#] Gregory M. Ferrence,[§] Matthias Zeller,[∥] Jeff W. Kampf,[‡] Vincent L. Pecoraro,*[,‡] and Curtis M. Zaleski*[,†]

[†]Department of Chemistry, Shippensburg University, 1871 Old Main Drive, Shippensburg, Pennsylvania 17257-2200, United States

[‡]Department of Chemistry, University of Michigan, 930 N. University Avenue, Ann Arbor, Michigan 48108-1005, United States

[§]Department of Chemistry, Illinois State University, Julian Hall 214, Normal, Illinois 61790-4160, United States

[∥]Department of Chemistry, Youngstown State University, WBSH 5053, Youngstown, Ohio 44555-0001, United States

[⊥]Department of Chemistry, Slippery Rock University, 1 Morrow Way, Slippery Rock, Pennsylvania 16057-1314, United States

Supporting Information

ABSTRACT: The inclusion of Ln^{III} ions into the 12-MC-4 framework generates the first heterotrimetallic complexes of this molecular class. The controllable and deliberate preparations of these compounds are demonstrated through 12 crystal structures of the $Ln^{III}M^{I}(OAc)_4[12\text{-}MC_{Mn^{III}(N)shi}\text{-}4](H_2O)_4\cdot 6DMF$ complex, where OAc^- is acetate, shi^{3-} is salicylhydroximate, and DMF is *N*,*N*-dimethylformamide. Compounds **1**−**12** have M^I as Na^I, and Ln^{III} can be Pr^{III} (**1**), Nd^{III} (**2**), Sm^{III} (**3**), Eu^{III} (**4**), Gd^{III} (**5**), Tb^{III} (**6**), Dy^{III} (**7**), Ho^{III} (**8**), Er^{III} (**9**), Tm^{III} (**10**), Yb^{III} (**11**), and Y^{III} (**12**). An example with $M^I = K^I$ and $Ln^{III} = Dy^{III}$ is also reported ($Dy^{III}K(OAc)_4[12\text{-}MC_{Mn^{III}(N)shi}\text{-}4](DMF)_4\cdot DMF$ (**14**)). When La^{III}, Ce^{III}, or Lu^{III} is used as the Ln^{III} ions to prepare the $Ln^{III}Na^{I}(OAc)_4[12\text{-}MC_{Mn^{III}(N)shi}\text{-}4]$ complex, the compound $Na_2(OAc)_2[12\text{-}MC_{Mn^{III}(N)shi}\text{-}4](DMF)_6\cdot 2DMF\cdot 1.60H_2O$ (**13**) results. For compounds **1**−**12**, the identity of the Ln^{III} ion affects the 12-$MC_{Mn^{III}(N)shi}$-4 framework as the largest Ln^{III}, Pr^{III}, causes an expansion of the 12-$MC_{Mn^{III}(N)shi}$-4 framework as demonstrated by the largest metallacrown cavity radius (0.58 Å for **1** to 0.54 Å for **11**), and the Pr^{III} causes the 12-$MC_{Mn^{III}(N)shi}$-4 framework to be the most domed structure as evident in the largest average angle about the axial coordination of the ring Mn^{III} ions (103.95° for **1** to 101.69° for **11**). For **14**, the substitution of K^I for Na^I does not significantly affect the 12-$MC_{Mn^{III}(N)shi}$-4 framework as many of the structural parameters such as the metallacrown cavity radius (0.56 Å) fall within the range of compounds **1**−**12**. However, the use of the larger K^I ion does cause the 12-$MC_{Mn^{III}(N)shi}$-4 framework to become more planar as evident in a smaller average angle about the axial coordination of the ring Mn^{III} ions (101.35°) compared to the analogous Dy^{III}/Na^I (**7**) complex (102.40°). In addition to broadening the range of structures available through the metallacrown analogy, these complexes allow for the mixing and matching of a diverse range of metals that might permit the fine-tuning of molecular properties where one day they may be exploited as magnetic materials or luminescent agents.

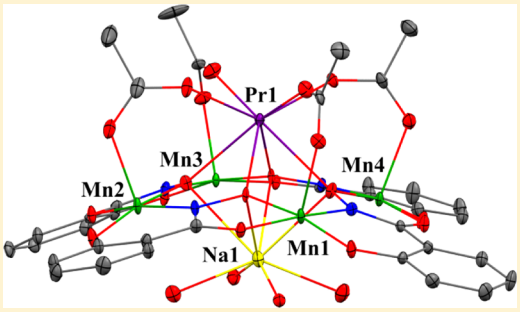

INTRODUCTION

The preparation and characterization of heterobimetallic systems has been reported for decades; however, the controllable preparation of heterotrimetallic systems has been less well-defined. Such centers are found in biology in enzymes such as the *Moorella thermoacetica* carbon monoxide dehydrogenase/acetyl CoA synthase (responsible for conversion of CO_2 to Acetyl-CoA) which contains an Fe_4S_4 unit linked to a heterobimetallic copper/nickel site.[1] Within the past decade several reports of heterotrimetallic coordination complexes and extended solids have appeared with exciting applications in molecular magnetism, luminescence, and catalysis.[2] Often, the complexes have contained lanthanides as one of the components of the mixture, and in some cases, the synthetic routes have proven general, allowing for the synthesis of series of related structures.

Since the recognition of metallacrowns (MC) in 1989, a variety of structures have been reported ranging in size from 9-MC-3 to 60-MC-20.[3] Most of these structures have shown the ability to encapsulate a central metal ion in the MC cavity, akin to crown ethers. Typically the central metal is a transition metal ion, though alkali, alkaline earth, and lanthanide metal ions have also been incorporated.[3,4] The first 12-MC-4, $Mn(OAc)_2[12\text{-}$

Received: November 18, 2013
Published: January 13, 2014

   dx.doi.org/10.1021/ic402865p | Inorg. Chem. 2014, 53, 1729−1742

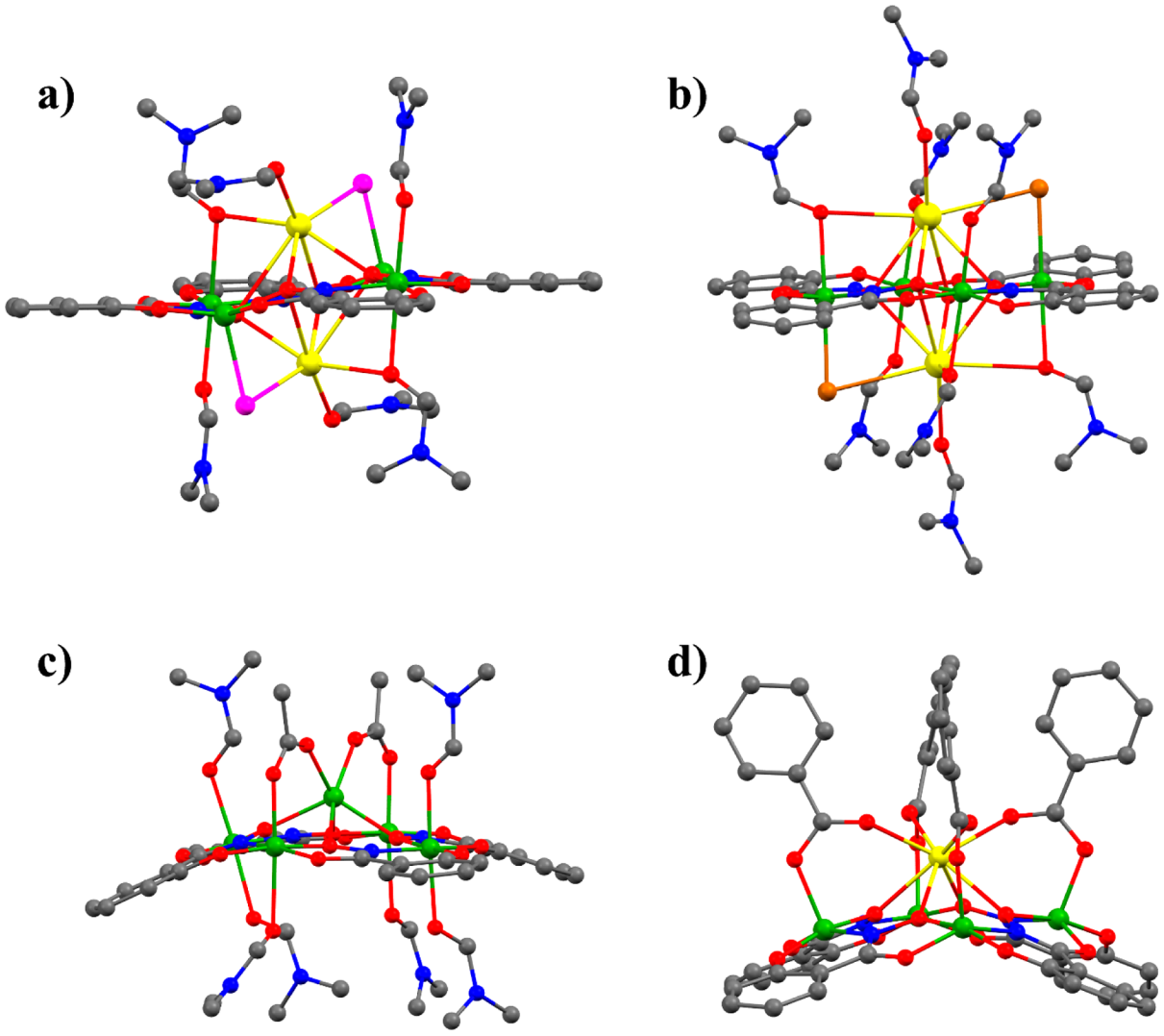

Figure 1. Single-crystal X-ray structures of previously reported M_mX_n[12-$MC_{Mn^{III}(N)shi}$-4] compounds (side views): (a) Na_2Cl_2[12-$MC_{Mn^{III}(N)shi}$-4];[6] (b) K_2Br_2[12-$MC_{Mn^{III}(N)shi}$-4];[6] (c) $Mn(OAc)_2$[12-$MC_{Mn^{III}(N)shi}$-4];[5] (d) Ca(benzoate)$_2$[12-$MC_{Mn^{III}(N)shi}$-4]$^{2-}$.[10] Color scheme: green, manganese; yellow, (a) Na^I, (b) K^I, (d) Ca^{II}; red, oxygen; blue, nitrogen; gray, carbon; pink, chloride; brown, bromide. Hydrogen atoms, lattice countercations, and lattice solvent molecules have been omitted for clarity.

$MC_{Mn^{III}(N)shi}$-4] where $^-$OAc is acetate and shi^{3-} is salicylhydroximate, was synthesized in 1989 by Lah and Pecoraro.[5] The molecule consisted of a -[Mn^{III}−N−O]- repeat unit with the triply deprotonated ligand salicylhydroximate and a Mn^{II} bound to the central cavity with the aid of two acetate bridges. Since then, the same MC framework (Mn^{III} and shi^{3-}) has been used to bind Li^I,[6] Na^I,[6−8] K^I,[6,8] and Ca^{II}[9,10] [although the Ca^{II} complex[10] was not identified as a 12-$MC_{Mn^{III}(N)shi}$-4 structure] in conjunction with various anions, and one 12-$MC_{Mn^{III}(N)shi}$-4 structure contains a Mn^{II} bound with benzoate bridges.[11] As shown in Figure 1, both the Na^I and K^I 12-$MC_{Mn^{III}(N)shi}$-4 structures bind two monovalent cations, which are slightly slipped to one edge of the four-atom oxime oxygen ring core of the macrocycle. These cations are stabilized by counteranions including chloride, bromide, and isothiocyanate.[6−8] Most interestingly, it was found that the Na^I and K^I complexes were preferred in the presence of halides and pseudohalides, but that in the presence of acetate, Mn^{II} formed the originally isolated mixed-valence species, $Mn(OAc)_2$[12-$MC_{Mn^{III}(N)shi}$-4]. Thus, it was demonstrated that cation affinity for the metallacrown was dependent on the bridging anionic ligands. Similarly, the affinity of the anions was dependent on the central cation.[8] Thus, the 12-$MC_{Mn^{III}(N)shi}$-4 entity could best be thought of as recognizing cation−anion pairs, rather than simply cations or anions. In 2008 a limited report of a Ln^{III}[12-$MC_{Mn^{III}(N)shi}$-4] complex with no structural details appeared in conference proceedings;[9] however, only larger metallacrown ring structures have bound lanthanide ions in the central cavity.[12−15] One report of a lanthanide (Tb^{III}) binding to a 12-MC-4 structure type containing Zn^{II} as the ring metal appeared as an $Tb^{III}Zn_{16}$ structure that formed a Tb^{III}[12-$MC_{Mn^{III}(N)picHA}$-4]$_2$ core, where H_2picHA= picoline hydroxamic acid, that was stabilized by a 24-$MC_{Zn^{II}(N)picHA}$-8 belt that bridged the two 12-MC-4 molecules.[16] In this case, the Tb^{III} was displaced out of the four oxygen atom plane formed by the 12-MC-4. This structure resulted in a tricationic species which contained lattice anions.

In addition to the fundamental insight that metallacrowns provide for understanding metallomacrocyclic chemistry, applications of these molecules in ion sensing,[6,8,14,17] lanthanide luminescence,[16] and molecular magnetism have been reported.[15,18] The mixture of lanthanide ions and transition

dx.doi.org/10.1021/ic402865p | Inorg. Chem. 2014, 53, 1729−1742

metals in compounds can lead to interesting magnetic properties such as single-molecule magnetism. Aside from probing the nature of 3d−4f electron interactions,[19] chemists have recently strived to combine these two types of ions to form single-molecule magnets (SMMs) in attempts to broaden the variety and better understand the phenomena of single-molecule magnetism.[20] In particular the combination of manganese and lanthanide ions has proved fruitful.[18,21] One key aspect of these molecules is to control the synthesis, design, and structural features of lanthanide−transition metal complexes. Metallacrowns are particularly suited for such studies as they allow facile substitution of central metals across a range of defined platforms such as 12-MC-4, 14-MC-5, and 15-MC-5 as well as other well-behaved polynuclear systems.[3] Since metallacrowns usually contain ring metals, central metals, and bridging anions, one may systematically vary each of these three components while retaining the basic structural topology of the system such as the $Ln^{III}(NO_3)_x[15\text{-}MC_{Cu^{II}(N)pheHA}\text{-}5](OH)_y$ system, where Ln^{III} = Y^{III} and La^{III}−Tm^{III} except Pm^{III}, pheHA = phenylalanine hydroxamic acid, and x = 1−3 and y = 3 − x.[22] In addition, the ability to control the structural features of the MC framework can lead to SMM behavior as evident for the first 12-MC-4, $Mn(OAc)_2[12\text{-}MC_{Mn^{III}(N)shi}\text{-}4]$,[18i] the first Mn−Ln SMM, Mn_6Ln_6,[18b] or the more recent 14-MC-5 SMMs, $Ln(OAc)_x[14\text{-}MC_{Mn^{III}4Ln^{III}(N)shi}\text{-}5]$.[15,18j] For both the 12-MC-4 and 14-MC-5 complexes, the planar nature of the MC allows the magnetoanisotropy vectors of the Mn^{III} to align, which contribute to the SMM behavior of the compound. Furthermore, the general MC framework has been used to produce other SMMs.[18]

Despite the numerous examples of heterobimetallic metallacrowns, a strategy to obtain heterotrimetallic assemblies using the metallacrown analogy has not been developed. Herein we report the synthetic schemes and structural descriptions of a new class of alkali metal−lanthanide−transition metal complexes, $Ln^{III}M^{I}(OAc)_4[12\text{-}MC_{Mn^{III}(N)shi}\text{-}4](H_2O)_4\cdot 6DMF$, where M^{I} being Na^{I}, Ln^{III} is Pr^{III}, Nd^{III}, Sm^{III}, Eu^{III}, Gd^{III}, Tb^{III}, Dy^{III}, Ho^{III}, Er^{III}, Tm^{III}, Yb^{III}, and Y^{III} (a transition metal ion with a radius that is close to that of the Ho^{III} [23]), and $Dy^{III}K(OAc)_4[12\text{-}MC_{Mn^{III}(N)shi}\text{-}4](DMF)_4\cdot DMF$, achieve this objective. The basic $Ln^{III}M^{I}(OAc)_4[12\text{-}MC_{Mn^{III}(N)shi}\text{-}4]^{4+}$ framework is presented in Scheme 1 with the MC ring highlighted and the acetates, which bridge the Ln^{III} and Mn^{III} ions, and solvent molecules that are bonded to M^{I} omitted for clarity. The presented Ln^{III} compounds expand the range of central cations complexed by the 12-MC-4 by providing the first example of a trivalent ion bound to this macrocycle. Furthermore, the inclusion of a monovalent countercation to the bottom of the ring allows for a fourth variable that may be altered when examining the physical properties of this system. This study proves the generality of the syntheses by demonstrating that different lanthanide ions and alkali ions can be easily substituted in the central cavity.

Scheme 1

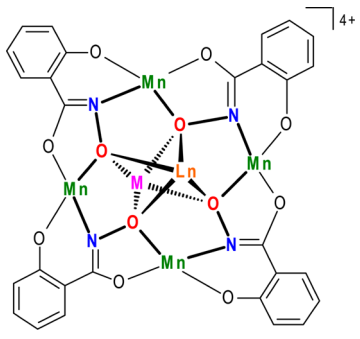

EXPERIMENTAL SECTION

Synthetic Materials. Lanthanum(III) nitrate hexahydrate (99.999%), terbium(III) nitrate pentahydrate (99.9%), and yttrium(III) nitrate hexahydrate (99.9%) were purchased from Sigma-Aldrich. Cerium(III) nitrate hexahydrate (99.5%), samarium(III) nitrate hexahydrate (99.9%), europium(III) nitrate hexahydrate (99.9%), gadolinium(III) nitrate hexhydrate (99.9%), and salicylhydroxamic acid (H_3shi, 99%) were purchased from Alfa Aesar. Praseodymium(III) nitrate hexahydrate (99.9%), neodymium(III) nitrate hexahydrate (99.9%), thulium(III) nitrate hexahydrate (99.9%), ytterbium(III) nitrate pentahydrate (99.9%), and lutetium(III) nitrate hydrate (99.9%) were purchased from Strem Chemicals. Dysprosium(III) nitrate pentahydrate (99.9%) was purchased from both Sigma-Aldrich and Alfa Aesar. Holmium(III) nitrate pentahydrate (99.9%) and erbium(III) nitrate pentahydrate (99.9%) were purchased from Acros Organics. Manganese(II) acetate tetrahydrate (99+%) was purchased from both Acros Organics and Sigma-Aldrich. Sodium acetate trihydrate (Certified ACS grade) and potassium hydroxide (Certified ACS grade, ≥85%) were purchased from Fisher Scientific. *N,N*-Dimethylformamide (DMF, Certified ACS grade) was purchased from both BDH Chemicals and Sigma-Aldrich. All reagents were used as received and without further purification.

Syntheses. *General Preparation of $Ln^{III}Na(OAc)_4[12\text{-}MC_{Mn^{III}(N)shi}\text{-}4](H_2O)_4\cdot 6DMF$ Compounds.* The lanthanide(III) nitrate hydrate salt (0.125 mmol), sodium acetate trihydrate (4 mmol), and salicylhydroxamic acid (2 mmol) were mixed in 10 mL of DMF resulting in a cloudy, slightly pink mixture. In a separate beaker, manganese(II) acetate tetrahydrate (2 mmol) was dissolved in 10 mL of DMF resulting in an orange/red solution. The two solutions were mixed resulting in a dark brown solution and then allowed to stir overnight. The solution was then filtered to remove a dark brown precipitate, which was discarded. Slow evaporation of the dark brown filtrate yielded X-ray quality cubic black/dark brown crystals after 1−8 weeks.

$Pr^{III}Na(OAc)_4[12\text{-}MC_{Mn^{III}(N)shi}\text{-}4](H_2O)_4\cdot 6DMF$, ***1***. The percent yield was 11% based on praseodymium(III) nitrate hexahydrate. Elemental analysis for $C_{54}H_{78}PrMn_4NaN_{10}O_{30}$ [fw = 1730.93 g/mol] found % (calculated): C = 37.44 (37.47), H = 4.39 (4.54), N = 8.00 (8.09). FT-IR bands (KBr pellet, cm^{-1}): 1654, 1600, 1572, 1550, 1514, 1436, 1395, 1322, 1258, 1249, 1154, 1100, 1024, 930, 867, 768, 755, 690, 649, 607, 539, 477.

$Nd^{III}Na(OAc)_4[12\text{-}MC_{Mn^{III}(N)shi}\text{-}4](H_2O)_4\cdot 6DMF$, ***2***. The percent yield was 60% based on neodymium(III) nitrate hexahydrate. Elemental analysis for $C_{54}H_{78}NdMn_4NaN_{10}O_{30}$ [FW = 1734.25 g/mol] found % (calculated): C = 37.34 (37.40), H = 4.42 (4.53), N = 8.06 (8.08). FT-IR bands (KBr pellet, cm^{-1}): 1651, 1600, 1573, 1551, 1514, 1436, 1395, 1321, 1258, 1249, 1155, 1101, 1025, 930, 867, 769, 755, 691, 650, 607, 536, 478.

$Sm^{III}Na(OAc)_4[12\text{-}MC_{Mn^{III}(N)shi}\text{-}4](H_2O)_4\cdot 6DMF$, ***3***. The percent yield was 27% based on samarium(III) nitrate hexahydrate. Elemental analysis for $C_{54}H_{78}SmMn_4NaN_{10}O_{30}$ [fw = 1740.36 g/mol] found % (calculated): C = 36.99 (37.27), H = 4.37 (4.52), N = 7.96 (8.05). FT-IR bands (KBr pellet, cm^{-1}): 1652, 1601, 1573, 1551, 1515, 1436, 1396, 1322, 1258, 1249, 1155, 1101, 1026, 931, 867, 768, 755, 691, 650, 608, 536, 478.

$Eu^{III}Na(OAc)_4[12\text{-}MC_{Mn^{III}(N)shi}\text{-}4](H_2O)_4\cdot 6DMF$, ***4***. The percent yield was 36% based on europium(III) nitrate hexahydrate. Elemental analysis for $C_{54}H_{78}EuMn_4NaN_{10}O_{30}$ [fw = 1741.97 g/mol] found % (calculated): C = 37.15 (37.23), H = 4.57 (4.51), N = 7.92 (8.04). FT-IR bands (KBr pellet, cm^{-1}): 1652, 1600, 1573, 1551, 1516, 1436, 1396, 1322, 1258, 1249, 1155, 1101, 1028, 931, 867, 768, 755, 691, 650, 609, 537, 478.

$Gd^{III}Na(OAc)_4[12\text{-}MC_{Mn^{III}(N)shi}\text{-}4](H_2O)_4\cdot 6DMF$, ***5***. The percent yield was 16% based on gadolinium(III) nitrate hexahydrate. Elemental

dx.doi.org/10.1021/ic402865p | *Inorg. Chem.* 2014, 53, 1729−1742

Table 1. Crystallographic Details for the $Ln^{III}Na(OAc)_4[12\text{-}MC_{Mn^{III}(N)shi}\text{-}4](H_2O)_4\cdot 6DMF$ Compounds (1−12) and $Na_2(OAc)_2[12\text{-}MC_{Mn^{III}(N)shi}\text{-}4](DMF)_6\cdot 2DMF\cdot 1.60H_2O$ (13)

	1	2	3	4	5
empirical formula	$C_{54}H_{78}PrMn_4NaN_{10}O_{30}$	$C_{54}H_{78}NdMn_4NaN_{10}O_{30}$	$C_{54}H_{78}SmMn_4NaN_{10}O_{30}$	$C_{54}H_{78}EuMn_4NaN_{10}O_{30}$	$C_{54}H_{78}GdMn_4NaN_{10}O_{30}$
fw (g/mol)	1730.93	1734.25	1740.36	1741.97	1747.26
T (K)	100(2)	100(2)	100(2)	100(2)	100(2)
wavelength (Å)	0.710 73	0.710 73	0.710 73	0.710 73	0.710 73
cryst syst	triclinic	triclinic	triclinic	triclinic	triclinic
space group	$P\bar{1}$	$P\bar{1}$	$P\bar{1}$	$P\bar{1}$	$P\bar{1}$
a (Å)	12.9551(8)	12.999(3)	12.9948(14)	12.9959(12)	13.0021(17)
b (Å)	16.0835(10)	16.108(3)	16.0950(17)	16.0915(15)	16.094(2)
c (Å)	17.5047(11)	17.471(3)	17.4377(19)	17.4147(16)	17.403(2)
α (deg)	89.280(3)	89.377(3)	89.3383(16)	89.3524(14)	89.367(2)
β (deg)	88.725(3)	88.793(3)	88.8405(16)	88.8596(14)	88.874(2)
γ (deg)	73.440(3)	73.224(3)	73.2931(15)	73.2486(13)	73.155(2)
V (Å^3)	3495.1(4)	3501.7(12)	3492.4(7)	3486.5(6)	3484.8(8)
Z	2	2	2	2	2
D (Mg/m^3) (calcd)	1.645	1.645	1.655	1.659	1.665
abs coeff (mm^{-1})	1.484	1.527	1.628	1.689	1.741
F(000)	1764	1766	1770	1772	1774
cryst size (mm^3)	0.550 × 0.400 × 0.090	0.330 × 0.260 × 0.041	0.390 × 0.320 × 0.070	0.340 × 0.300 × 0.060	0.420 × 0.390 × 0.100
θ range for data collection (deg)	1.164−30.507	2.332−31.267	2.380−31.497	2.644−31.530	1.637−30.999
limiting indices	$-18 \le h \le 18, -22 \le k \le 22, 0 \le l \le 24$	$-18 \le h \le 18, -23 \le k \le 23, 0 \le l \le 24$	$-18 \le h \le 18, -23 \le k \le 23, 0 \le l \le 24$	$-18 \le h \le 18, -23 \le k \le 23, 0 \le l \le 25$	$-18 \le h \le 18, -23 \le k \le 23, -25 \le l \le 25$
reflns collected/ unique	56 472/28 211 [R(int) = 0.0564]	35 704/20 209 [R(int) = 0.0541]	33 305/20 450 [R(int) = 0.0329]	35 104/21 010 [R(int) = 0.0386]	37 851/21 267 [R(int) = 0.0320]
max and min transm	0.7478 and 0.5434	0.7462 and 0.5819	0.7462 and 0.5690	0.7462 and 0.5843	0.7463 and 0.6070
data/restraints/ params	28 211/8/979	20 209/58/978	20 450/40/984	21 010/40/984	21 267/8/979
GOF of F^2	1.065	1.022	1.046	1.054	1.082
final R indices [$I > 2\sigma(I)$]	R1[a] = 0.0446, wR2[b] = 0.1169	R1[a] = 0.0365, wR2[b] = 0.0758	R1[a] = 0.0250, wR2[b] = 0.0615	R1[a] = 0.0243, wR2[b] = 0.0597	R1[a] = 0.0262, wR2[b] = 0.0610
R indices (all data)	R1[a] = 0.0569, wR2[b] = 0.1305	R1[a] = 0.0503, wR2[b] = 0.0815	R1[a] = 0.0293, wR2[b] = 0.0642	R1[a] = 0.0279, wR2[b] = 0.0626	R1[a] = 0.0319, wR2[b] = 0.0648
largest diff peak and hole (e$^-$ Å^{-3})	2.092 and −1.713	1.091 and −0.665	1.250 and −0.564	1.330 and −0.648	0.873 and −0.689

	6	7	8	9	10
empirical formula	$C_{54}H_{78}TbMn_4NaN_{10}O_{30}$	$C_{54}H_{78}DyMn_4NaN_{10}O_{30}$	$C_{54}H_{78}HoMn_4NaN_{10}O_{30}$	$C_{54}H_{78}ErMn_4NaN_{10}O_{30}$	$C_{54}H_{78}TmMn_4NaN_{10}O_{30}$
fw (g/mol)	1748.93	1752.51	1754.94	1757.27	1758.94
T (K)	100(2)	100(2)	100(2)	100(2)	100(2)
wavelength (Å)	0.710 73	0.710 73	0.710 73	0.710 73	0.710 73
cryst syst	triclinic	triclinic	triclinic	triclinic	triclinic
space group	$P\bar{1}$	$P\bar{1}$	$P\bar{1}$	$P\bar{1}$	$P\bar{1}$
a (Å)	12.9813(4)	12.9657(13)	12.9749(9)	12.9903(14)	12.980(3)
b (Å)	16.0778(5)	16.0684(16)	16.0760(11)	16.0769(17)	16.066(4)
c (Å)	17.3885(5)	17.4114(16)	17.3795(12)	17.3630(18)	17.333(4)
α (deg)	89.3690(10)	89.412(5)	89.404(4)	89.395(2)	89.392(3)
β (deg)	88.871(2)	88.862(5)	88.872(4)	88.890(2)	88.886(3)
γ (deg)	73.2570(10)	73.308(5)	73.320(4)	73.224(2)	73.237(3)
V (Å^3)	3474.59(18)	3473.9(6)	3471.8(4)	3471.1(6)	3460.2(13)
Z	2	2	2	2	2
D (Mg/m^3) (calcd)	1.672	1.675	1.679	1.681	1.688
abs coeff (mm^{-1})	1.810	1.867	1.932	2.001	2.077
F(000)	1776	1778	1780	1782	1784
cryst size (mm^3)	0.550 × 0.400 × 0.090	0.390 × 0.200 × 0.090	0.250 × 0.200 × 0.050	0.360 × 0.120 × 0.030	0.310 × 0.190 × 0.060
θ range for data collection (deg)	1.638−31.991	1.170−32.030	1.322−32.027	2.346−30.893	2.385−31.398
limiting indices	$-19 \le h \le 19, -23 \le k \le 23, 0 \le l \le 25$	$-19 \le h \le 19, -23 \le k \le 23, 0 \le l \le 25$	$-19 \le h \le 19, -23 \le k \le 23, 0 \le l \le 25$	$-18 \le h \le 18, -23 \le k \le 23, 0 \le l \le 25$	$-18 \le h \le 18, -22 \le k \le 23, 0 \le l \le 24$
reflns collected/ unique	160 910/22 218 [R(int) = 0.0327]	153 453/22 105 [R(int) = 0.0388]	22 427/22 427 [R(int) = 0.0351]	35 210/20 276 [R(int) = 0.0441]	35 899/19 791 [R(int) = 0.0486]
max and min transm	0.7463 and 0.5827	0.7463 and 0.6161	0.7463 and 0.6155	0.7461 and 0.5819	0.7462 and 0.5805
data/restraints/ params	22 218/8/979	22 105/8/982	22 427/8/981	20 276/40/984	19 791/40/984

dx.doi.org/10.1021/ic402865p | Inorg. Chem. 2014, 53, 1729−1742

Table 1. continued

	6	7	8	9	10
GOF of F^2	1.111	1.085	1.043	1.023	1.026
final R indices [$I > 2\sigma(I)$]	R1[a] = 0.0237, wR2[b] = 0.0568	R1[a] = 0.0243, wR2[b] = 0.0502	R1[a] = 0.0225, wR2[b] = 0.0494	R1[a] = 0.0295, wR2[b] = 0.0647	R1[a] = 0.0350, wR2[b] = 0.0686
R indices (all data)	R1[a] = 0.0288, wR2[b] = 0.0604	R1[a] = 0.0331, wR2[b] = 0.0544	R1[a] = 0.0278, wR2[b] = 0.0519	R1[a] = 0.0361, wR2[b] = 0.0678	R1[a] = 0.0486, wR2[b] = 0.0737
largest diff peak and hole (e^- Å^{-3})	1.686 and −1.074	1.789 and −0.817	1.530 and −0.581	1.230 and −0.670	1.424 and −0.999

	11	12	13
empirical formula	$C_{54}H_{78}YbMn_4NaN_{10}O_{30}$	$C_{54}H_{78}YMn_4NaN_{10}O_{30}$	$C_{56}H_{81.20}Mn_4N_{12}Na_2O_{25.60}$
fw (g/mol)	1763.05	1678.92	1597.94
T (K)	100(2)	100(2)	100(2)
wavelength (Å)	0.710 73	0.710 73	0.710 73
cryst syst	triclinic	triclinic	monoclinic
space group	$P\bar{1}$	$P1$	$P2_1/c$
a (Å)	12.9978(11)	12.9998(10)	14.8397(14)
b (Å)	16.0779(13)	16.0840(12)	17.1527(16)
c (Å)	17.3428(14)	17.3773(13)	14.7756(14)
α (deg)	89.4135(12)	89.4150(10)	90
β (deg)	88.8742(12)	88.8920(10)	111.4680(10)
γ (deg)	73.2204(12)	73.1890(10)	90
V (Å^3)	3469.2(5)	3477.4(5)	3500.1(6)
Z	2	2	2
D (Mg/m^3) (calcd)	1.688	1.603	1.516
abs coeff (mm^{-1})	2.141	1.630	0.804
F(000)	1786	1724	1656
cryst size (mm^3)	0.210 × 0.120 × 0.030	0.400 × 0.310 × 0.050	0.450 × 0.430 × 0.390
θ range for data collection (deg)	2.154−31.470	2.152−30.326	2.375−31.412
limiting indices	$-18 \le h \le 18$, $-23 \le k \le 23$, $0 \le l \le 24$	$-18 \le h \le 18$, $-22 \le k \le 22$, $-24 \le l \le 24$	$-21 \le h \le 21$, $-24 \le k \le 25$, $-21 \le l \le 21$
reflns collected/unique	48 628/36391 [R(int) = 0.0420]	161 036/56 304 [R(int) = 0.0431]	74 616/10 855 [R(int) = 0.0244]
max and min transm	0.7462 and 0.5549	0.7460 and 0.5001	0.7462 and 0.6373
data/restraints/params	36 391/40/984	56 304/75/1319	10 855/24/532
GOF of F^2	1.035	1.039	1.039
final R indices [$I > 2\sigma(I)$]	R1[a] = 0.0271, wR2[b] = 0.0633	R1[a] = 0.0402, wR2[b] = 0.0928	R1[a] = 0.0290, wR2[b] = 0.0758
R indices (all data)	R1[a] = 0.0329, wR2[b] = 0.0660	R1[a] = 0.0532, wR2[b] = 0.0996	R1[a] = 0.0353, wR2[b] = 0.0815
largest diff peak and hole (e^- Å^{-3})	1.116 and −0.632	0.921 and −0.882	0.586 and −0.307

[a] $R1 = \Sigma(||F_o| - |F_c||)/\Sigma|F_o|$. [b] $wR2 = [\Sigma[w(F_o^2 - F_c^2)^2]/\Sigma[w(F^o)^2]]^{1/2}$; $w = 1/[\sigma^2(F_o^2) + (mp)^2 + np]$; $p = [\max(F_o^2,0) + 2F_c^2]/3$ (m and n are constants); $\sigma = [\Sigma[w(F_o^2 - F_c^2)^2]/(n - p)]^{1/2}$.

analysis for $C_{54}H_{78}GdMn_4NaN_{10}O_{30}$ [fw = 1747.26 g/mol] found % (calculated): C = 37.50 (37.12), H = 4.23 (4.50), N = 7.71 (8.02). FT-IR bands (KBr pellet, cm^{-1}): 1653, 1601, 1573, 1552, 1515, 1436, 1395, 1321, 1258, 1248, 1155, 1101, 1027, 931, 867, 768, 755, 691, 650, 609, 536, 479.

$Tb^{III}Na(OAc)_4$[12-$MC_{Mn^{III}(N)shi}$-4]$(H_2O)_4$·6DMF, **6**. The percent yield was 28% based on terbium(III) nitrate pentahydrate. Elemental analysis for $C_{54}H_{78}TbMn_4NaN_{10}O_{30}$ [fw = 1748.93 g/mol] found % (calculated): C = 37.31 (37.08), H = 4.37 (4.50), N = 7.74 (8.01). FT-IR bands (KBr pellet, cm^{-1}): 1653, 1601, 1573, 1552, 1515, 1436, 1396, 1322, 1258, 1248, 1156, 1101, 1028, 932, 867, 769, 755, 691, 651, 610, 537, 480.

$Dy^{III}Na(OAc)_4$[12-$MC_{Mn^{III}(N)shi}$-4]$(H_2O)_4$·6DMF, **7**. The percent yield was 45% based on dysprosium(III) nitrate hydrate. Elemental analysis for $C_{54}H_{78}DyMn_4NaN_{10}O_{30}$ [fw = 1752.51 g/mol] found % (calculated): C = 37.23 (37.01), H = 4.52 (4.49), N = 7.84 (7.99). FT-IR bands (KBr pellet, cm^{-1}): 1654, 1600, 1574, 1552, 1514, 1435, 1392, 1316, 1256, 1244, 1156, 1100, 1028, 931, 865, 770, 755, 689, 651, 613, 535, 483.

$Ho^{III}Na(OAc)_4$[12-$MC_{Mn^{III}(N)shi}$-4]$(H_2O)_4$·6DMF, **8**. The percent yield was 22% based on holmium(III) nitrate pentahydrate. Elemental analysis for $C_{54}H_{78}HoMn_4NaN_{10}O_{30}$ [fw = 1754.94 g/mol] found % (calculated): C = 37.00 (36.96), H = 4.40 (4.48), N = 7.77 (7.98). FT-IR bands (KBr pellet, cm^{-1}): 1653, 1601, 1573, 1552, 1516, 1437, 1396, 1322, 1258, 1248, 1155, 1101, 1029, 932, 867, 768, 755, 691, 651, 610, 535, 480.

$Er^{III}Na(OAc)_4$[12-$MC_{Mn^{III}(N)shi}$-4]$(H_2O)_4$·6DMF, **9**. The percent yield was 83% based on erbium(III) nitrate pentahydrate. Elemental analysis for $C_{54}H_{78}ErMn_4NaN_{10}O_{30}$ [fw = 1757.27 g/mol] found % (calculated): C = 36.79 (36.91), H = 4.53 (4.47), N = 7.95 (7.97). FT-IR bands (KBr pellet, cm^{-1}): 1653, 1601, 1574, 1553, 1517, 1437, 1396, 1322, 1258, 1248, 1155, 1101, 1030, 932, 867, 768, 755, 691, 651, 610, 536, 479.

$Tm^{III}Na(OAc)_4$[12-$MC_{Mn^{III}(N)shi}$-4]$(H_2O)_4$·6DMF, **10**. The percent yield was 18% based on thulium(III) nitrate hexahydrate. Elemental analysis for the dried material $C_{54}H_{78}TmMn_4NaN_{10}O_{30}$ [fw = 1758.94 g/mol] found % (calculated): C = 36.01 (36.87), H = 4.14 (4.47), N = 7.49 (7.96). FT-IR bands (KBr pellet, cm^{-1}): 1652, 1599, 1574, 1555, 1514, 1436, 1394, 1319, 1257, 1247, 1158, 1101, 1030, 932, 866, 774, 758, 689, 651, 615, 538, 481.

$Yb^{III}Na(OAc)_4$[12-$MC_{Mn^{III}(N)shi}$-4]$(H_2O)_4$·6DMF, **11**. The percent yield was 11% based on ytterbium(III) nitrate pentahydrate. Elemental analysis for $C_{54}H_{78}YbMn_4NaN_{10}O_{30}$ [fw = 1763.05 g/mol] found % (calculated): C = 36.25 (36.79), H = 4.32 (4.46), N = 7.62 (7.94). FT-IR bands (KBr pellet, cm^{-1}): 1653, 1601, 1574, 1553, 1518, 1438, 1396, 1322, 1258, 1248, 1156, 1102, 1032, 932, 867, 769, 755, 692, 652, 612, 539, 480.

dx.doi.org/10.1021/ic402865p | Inorg. Chem. 2014, 53, 1729−1742

$Y^{III}Na(OAc)_4[12\text{-}MC_{Mn^{III}(N)shi}\text{-}4](H_2O)_4\cdot 6DMF$, **12**. The percent yield was 7.3% based on yttrium(III) nitrate hexahydrate. Elemental analysis for $C_{54}H_{78}YMn_4NaN_{10}O_{30}$ [fw = 1678.92 g/mol] found % (calculated): C = 38.20 (38.63), H = 4.40 (4.68), N = 7.64 (8.34). FT-IR bands (KBr pellet, cm^{-1}): 1652, 1601, 1573, 1555, 1516, 1436, 1395, 1321, 1258, 1248, 1156, 1101, 1030, 932, 867, 768, 755, 691, 651, 611, 538, 481.

Preparation of $Na_2(OAc)_2[12\text{-}MC_{Mn^{III}(N)shi}\text{-}4](DMF)_6\cdot 2DMF\cdot 1.60H_2O$. *$Na_2(OAc)_2[12\text{-}MC_{Mn^{III}(N)shi}\text{-}4](DMF)_6\cdot 2DMF\cdot 1.60H_2O$*, **13**. Sodium acetate trihydrate (4 mmol) and salicylhydroxamic acid (2 mmol) were mixed in 10 mL of DMF resulting in a cloudy, slightly pink mixture. In a separate beaker, manganese(II) acetate tetrahydrate (2 mmol) was dissolved in 10 mL of DMF resulting in an orange/red solution. The two solutions were mixed resulting in a dark brown solution and then allowed to stir overnight. Following this, the solution was filtered to remove a dark brown precipitate, which was discarded. Slow evaporation of the dark brown filtrate yielded X-ray quality cubic black/dark brown crystals after 6 days. The percent yield was 53% based on manganese(II) acetate tetrahydrate. Elemental analysis for $C_{56}H_{81.20}Mn_4Na_2N_{12}O_{25.60}$ [fw = 1597.94 g/mol] found % (calculated): C = 42.23 (42.09), H = 5.17 (5.12), N = 10.40 (10.52). FT-IR bands (KBr pellet, cm^{-1}): 1656, 1599, 1568, 1511, 1469, 1434, 1390, 1315, 1256, 1156, 1144, 1098, 1032, 935, 863, 756, 680, 649, 612, 585, 542, 479.

If 0.125 mmol of lanthanum(III) nitrate hexahydrate, cerium(III) nitrate hexahydrate, or lutetium(III) nitrate hydrate is included in the synthesis as described for compounds **1**−**12**, the respective lanthanide ion is not incorporated into the metallacrown and compound **13** is synthesized instead.

Preparation of $Dy^{III}K(OAc)_4[12\text{-}MC_{Mn^{III}(N)shi}\text{-}4](DMF)_4\cdot DMF$. *$Dy^{III}K(OAc)_4[12\text{-}MC_{Mn^{III}(N)shi}\text{-}4](DMF)_4\cdot DMF\cdot 2K(Hsal)$*, **14**. Manganese(II) acetate tetrahydrate (4 mmol) and potassium hydroxide (2.7 mmol) were dissolved in 15 mL of DMF. In a separate beaker, salicylhydroxamic acid (4 mmol) and dysprosium(III) nitrate pentahydrate (0.5 mmol) were dissolved in 16 mL of DMF. After the manganese acetate/potassium hydroxide solution turned red in color, it was added to the dysprosium(III) nitrate/salicylhydroxamic acid solution resulting in a dark green-brown solution; this solution was then allowed to stir overnight. Following this, the solution was filtered, and the dark green-brown filtrate was divided into multiple small 20 mL scintillation vials to allow slow evaporation of the solvent. X-ray quality green block crystals were isolated after 5 months. The percent yield was 5.9% based on dysprosium(III) nitrate pentahydrate. Due to the extended period of time necessary to crystallize the metallacrown, potassium salicylate ($C_7H_5KO_3$) also cocrystallized with the metallacrown. Efforts were made to separate the compounds; however, complete separation could not be achieved. Thus, the elemental analysis percentages take into account the potassium salicylate. Elemental analysis for $C_{51}H_{63}DyMn_4KN_9O_{25}\cdot 2KC_7H_5O_3$ [fw = 1975.864 g/mol] found % (calculated) C = 39.87 (39.51), H = 3.92 (3.72), N = 6.74 (6.38).

Physical Methods. FT-IR spectra were obtained on a Jasco FT-IR 460 Plus spectrometer. Elemental analyses were performed on a Carlo Erba 1108 elemental analyzer and a PerkinElmer 2400 elemental analyzer.

X-ray Crystallography. For compounds **1**−**13**, a mineral oil coated crystal was mounted on a MicroMesh MiTeGen Micromount and transferred to a Bruker AXS SMART APEXII CCD X-ray diffractometer. The X-ray diffraction data were collected at 100 K using Mo Kα (λ = 0.710 73 Å) radiation. Data collection and cell refinement were performed using APEX2 (Bruker AXS Inc., Madison, Wisconsin, 2012) and SAINT+ (Bruker) embedded in APEX2, respectively. Additional details are provided in Table 1 and in the individual CIFs of each compound.

For compound **14**, crystals were mounted onto a standard Bruker APEX-I CCD-based X-ray diffractometer equipped with a low temperature device. The X-ray diffraction data were collected at 85 K using Mo Kα (λ = 0.710 73 Å) radiation. Data collection and cell refinement were performed using SMART (Bruker, APEX-I) and SAINT+ (Bruker), respectively. Additional details are provided in Table 2 and in the individual CIF of the compound.

Table 2. Crystallographic Details for $Dy^{III}K(OAc)_4[12\text{-}MC_{Mn^{III}(N)shi}\text{-}4](DMF)_4\cdot DMF$ (14)

	14
empirical formula	$C_{63}H_{51}DyMn_4KN_9O_{25}$
fw (g/mol)	1623.46
T (K)	85(2)
wavelength (Å)	0.710 73
cryst syst	monoclinic
space group	$C2/c$
a (Å)	16.1208(13)
b (Å)	16.3127(13)
c (Å)	23.4413(18)
α (deg)	90.00
β (deg)	95.3460(10)
γ (deg)	90.00
V (Å^3)	6137.6(8)
Z	4
D (Mg/m^3) (calcd)	1.757
abs coeff (mm^{-1})	2.160
F(000)	3268
crystal size (mm)	0.28 × 0.10 × 0.09
θ range for data collection (deg)	1.75−28.34
limiting indices	$-21 \le h \le 21$, $-21 \le k \le 21$, $-31 \le l \le 31$
reflns collected/unique	85 865/7659 [R(int) = 0.0452]
max and min transm	0.8293 and 0.5830
data/restraints/params	7659/438/0
GOF of F^2	1.096
final R indices [$I > 2\sigma(I)$]	R1[a] = 0.0328, wR2[b] = 0.0854
R indices (all data)	R1[a] = 0.0373, wR2[b] = 0.0882
largest diff peak and hole (e$^-$ Å^{-3})	0.981 and −0.922

[a] $R1 = \Sigma(||F_o| - |F_c||)/\Sigma|F_o|$. [b] $wR2 = [\Sigma[w(F_o^2 - F_c^2)^2]/\Sigma[w(F^{o})^2]]^{1/2}$; $w = 1/[\sigma^2(F_o^2) + (mp)^2 + np]$; $p = [\max(F_o^2,0) + 2F_c^2]/3$ (m and n are constants); $\sigma = [\Sigma[w(F_o^2 - F_c^2)^2]/(n - p)]^{1/2}$.

RESULTS

General Description of $Ln^{III}Na(OAc)_4[12\text{-}MC_{Mn^{III}(N)shi}\text{-}4](H_2O)_4\cdot 6DMF$ Structures. Each metallacrown (**1**−**12**) consists of the typical 12-$MC_{Mn^{III}(N)shi}$-4 framework (Figure 2 and Supporting Information Figures S1−S24). A pseudo-C_4 axis is located in the MC central cavity, which produces a Mn−N−O repeat unit that occurs four times to complete a square geometry. A lanthanide ion and a sodium ion are bound on opposite faces of the central cavity (Figure 2b).

The metallacrown is slightly domed with the lanthanide ion captured on the convex side of the central cavity, while a sodium ion is captured on the concave side (underside) of the central cavity. Each Mn and Ln is assigned an oxidation state of 3+. This is supported by the bond valence sum calculations and average bond lenghs (Supporting Information Table S1).[24] In addition, charge considerations support the oxidation states of the metal ions. The presence of four $^-$OAc and four shi^{3-} ligands provides 16 negative charges that are balanced by four Mn^{III}, one Ln^{III}, and one Na^{I}. Each Mn^{III} ion could be considered to be five coordinate with a slightly distorted square pyramidal geometry and an elongated axis approximately perpendicular to the plane of the metallacrown. This geometry assignment is supported by τ values[25] near zero (Supporting

dx.doi.org/10.1021/ic402865p | Inorg. Chem. 2014, 53, 1729−1742

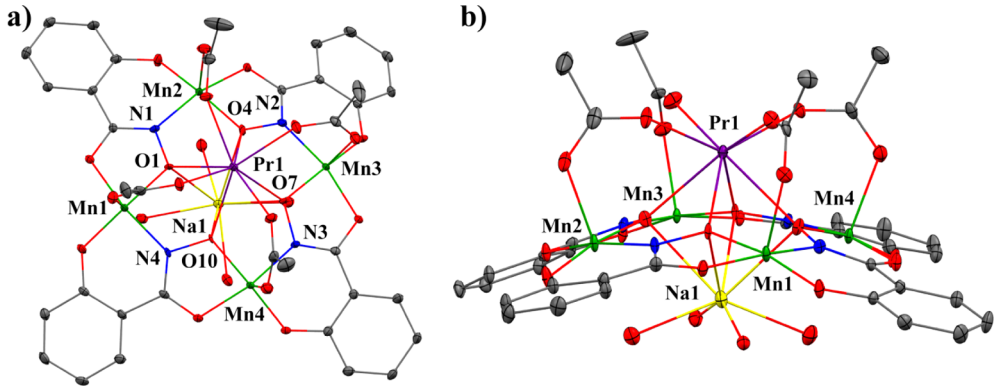

Figure 2. Single-crystal X-ray structure of $Pr^{III}Na(OAc)_4[12\text{-}MC_{Mn^{III}(N)shi}\text{-}4](H_2O)_4\cdot 6DMF$, **1**: (a) top view and (b) side view. The thermal ellipsoid plot of **1** is at 50% probability level. All atoms comprising the MC ring are labeled in part a, and only the metal atoms are labeled in part b. Hydrogen atoms and the lattice solvent molecules have been omitted for clarity. Color scheme: purple, Pr^{III}; green, Mn^{III}; yellow, Na^{I}; red, oxygen; blue, nitrogen; gray, carbon.

Information Table S2) in which an ideal square pyramidal geometry is given by $\tau = 0$ and an ideal trigonal bipyramidal geometry is specified as $\tau = 1$. The basal atoms of the coordination are supplied by the oxime and carbonyl oxygen atoms of one shi^{3-} to form a five-membered chelate ring and a six-membered chelate ring formed on the opposite side by the oxime nitrogen and phenolate oxygen atoms of a second shi^{3-}. An oxygen atom from a bridging acetate anion serves as the apical ligand. The acetate anion bridges each ring Mn^{III} to the central Ln^{III}. An alternative description of the Mn^{III} polyhedron is that of a highly tetragonally distorted 6-coordinate complex with very long Mn−water distances (~2.5 Å). As discussed below, these water molecules are also bound to the Na^{I} ion, which could lead to these longer distances especially in a Jahn−Teller system where a neutral ligand is *trans* to an anion. Additionally, the water−Mn−acetate oxygen bond angles closely approximate 180° (173.5−177.6° for **1**).

Each Ln^{III} is eight coordinate with a slightly distorted square antiprismatic geometry as shown for **1** in Figure 3. The bridging

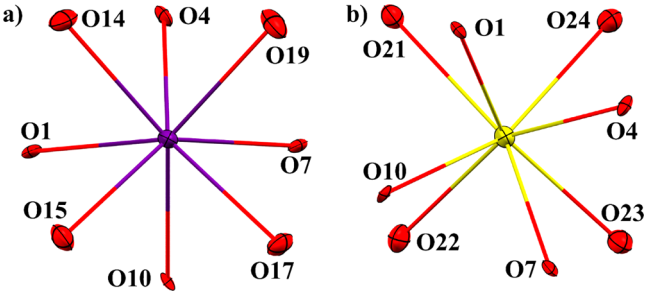

Figure 3. (a) View of the first coordination sphere of Pr^{III} (purple) in **1** along the pseudo-C_4 axis illustrating the square antiprismatic geometry of the 8-coordinate lanthanide ion. (b) View of the first coordination sphere of Na^{I} (yellow) in **1** along the pseudo-C_4 axis showing the significant distortion from square antiprismatic geometry. For both (a) and (b) the MC ring oxime oxygen atoms are O1, O4, O7, and O10. The thermal ellipsoid plot is at 50% probability level.

acetates provide four oxygen atoms, while the Ln^{III} binds to the central cavity of the MC via the oxime oxygen atoms of the shi^{3-} ligands. The assignment of square antiprismatic geometry about the Ln^{III} is supported by calculated skew angles (Φ) about the Ln^{III} (Supporting Information Table S3) which are near 45°.[26] For an ideal square prism geometry Φ = 0°, and for an ideal square antiprism geometry Φ = 45°. The skew angles were calculated using the program *Mercury*[27] by defining the centroids of the acetate oxygen atoms and oxime oxygen atoms and then measuring the angle about the Ln^{III} (Supporting Information Figure S25).

The octacoordinate Na^{I} ion binds to the central cavity of the MC with the oxime oxygen atoms of the shi^{3-} ligands, and the coordination is completed by four water molecules. The top four oxime oxygen atoms and bottom four water oxygen atoms form a severely distorted square antiprism geometry about the Na^{I} as shown in Figure 3. The geometry assignment is supported by calculated skew angles (Φ) about the Na^{I} as the angle is between that of both ideal values (Supporting Information Table S3). The skew angles were again calculated using the program *Mercury* with the same procedure stated for the Ln^{III} ions (Supporting Information Figure S26).

The Pr^{III} and Na^{I} ions are displaced from the centroid of their respective polyhedra away from the metallacrown ring oxime oxygen atoms as best seen in Figure 4 and tabulated in

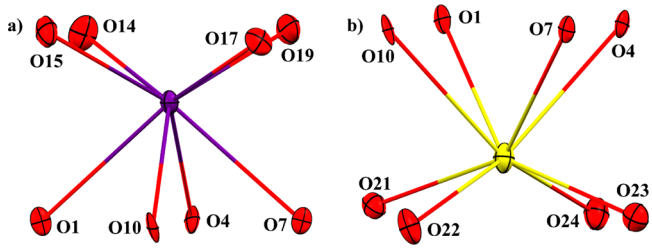

Figure 4. Illustration (side views) of the displacement in **1** of the Pr^{III} ion (a) and Na^{I} ion (b) from the center of the polyhedron that surround the metals. The movement in both cases is away from the metallacrown ring oxime oxygen atoms (O1, O4, O7, O10). In part a, the oxime oxygen atoms are located on the bottom, while in part b the oxime oxygen atoms are located on the top. The thermal ellipsoid plot is at 50% probability level.

Table 3. In **1**, the Pr^{III} is 1.70 Å from the oxime oxygen mean plane ($O_{ox}MP$), while it is displaced 0.97 Å from the corresponding mean plane made from the four oxygen atoms of the bridging acetates ($O_{ac}MP$). This corresponds to a 0.37 Å displacement of the Pr^{III} away from the metallacrown ring toward the acetate oxygen atoms. Similarly, the Na^{I} cation is slightly further removed from the $O_{ox}MP$ (1.88 Å), while being 0.82 Å from the mean plane produced by the four oxygen water

dx.doi.org/10.1021/ic402865p | *Inorg. Chem.* 2014, 53, 1729−1742

Table 3. Structural Feature Comparison of the Ln^{III}[12-$MC_{Mn^{III}(N)shi}$-4] Structures

compd	Ln^{III} crystal radius (Å)[a]	alkali metal crystal radius (Å)[a]	MC cavity radius (Å)[b]	av adjacent Mn^{III}–Mn^{III} distance (Å)	av cross cavity Mn^{III}–Mn^{III} distance (Å)
1	1.15	1.24	0.58	4.63	6.54
2	1.14	1.25	0.57	4.62	6.54
3	1.11	1.24	0.57	4.62	6.53
4	1.10	1.24	0.56	4.62	6.53
5	1.09	1.25	0.56	4.62	6.53
6	1.07	1.24	0.56	4.61	6.52
7	1.06	1.24	0.55	4.61	6.52
8	1.05	1.24	0.55	4.61	6.52
9	1.04	1.24	0.55	4.61	6.51
10	1.03	1.24	0.55	4.60	6.51
11	1.03	1.24	0.54	4.61	6.51
12_A	1.05	1.24	0.55	4.61	6.52
12_B	1.05	1.24	0.55	4.61	6.52
13	N/A	1.15	0.55	4.62	6.54
14	1.06	1.50	0.56	4.63	6.54

compd	av cross cavity O_{ox}-O_{ox} distance (Å)	av cross cavity O_{ac}-O_{ac} distance (Å)	av cross cavity $O_{solvent}$-$O_{solvent}$ distance (Å)
1	3.75	4.32	4.58
2	3.74	4.28	4.57
3	3.73	4.21	4.58
4	3.72	4.17	4.58
5	3.72	4.15	4.58
6	3.71	4.11	4.58
7	3.71	4.08	4.58
8	3.70	4.05	4.58
9	3.69	4.02	4.58
10	3.70	3.99	4.58
11	3.69	3.98	4.58
12_A	3.70	4.04	4.58
12_B	3.70	4.05	4.58
13	3.71	N/A	N/A
14	3.71	4.00	5.33

compd	Ln^{III}–O_{ox}MP distance (Å)	Ln^{III}–O_{ac}MP distance (Å)	Ln^{III}–MnMP distance (Å)	Ln^{III} distance difference between MnMP and O_{ox}MP (Å)
1	1.70	0.97	2.07	0.37
2	1.68	0.99	2.05	0.36
3	1.65	1.00	2.01	0.36
4	1.63	1.02	1.99	0.36
5	1.62	1.03	1.97	0.35
6	1.61	1.02	1.96	0.35
7	1.59	1.03	1.94	0.35
8	1.58	1.03	1.92	0.35
9	1.57	1.04	1.91	0.35
10	1.56	1.03	1.91	0.35
11	1.55	1.03	1.90	0.35
12_A	1.57	1.04	1.92	0.35
12_B	1.58	1.03	1.93	0.35
13	N/A	N/A	N/A	N/A
14	1.59	1.07	1.86	0.27

compd	Na^+ or K^+–O_{ox}MP distance (Å)	Na^+ or K^+–$O_{solvent}$MP distance (Å)	Ln^{III}–Na^+ or K^+ distance (Å)
1	1.88	0.82	3.58
2	1.89	0.82	3.58
3	1.89	0.81	3.54
4	1.90	0.80	3.53
5	1.91	0.80	3.53
6	1.90	0.80	3.51
7	1.90	0.80	3.50
8	1.91	0.79	3.49
9	1.91	0.79	3.48
10	1.91	0.80	3.46
11	1.91	0.79	3.46
12_A	1.92	0.79	3.49
12_B	1.91	0.79	3.49
13	1.66	N/A	3.34
14	2.21	0.50	3.80

[a]The Ln^{III} crystal radius was calculated by determining the average Ln^{III}–O bond distance and then subtracting the estimated radius of an oxygen atom (1.30 Å). A similar method was used to calculate the Na^I and K^I crystal radii. [b]The metallacrown cavity radius was calculated according to the method described in Supporting Information Figure S30. First the average oxime oxygen distance was determined about the MC ring, and then this distance was used to determine the distance from the oxime oxygen atom to the center of the MC ring. The MC cavity radius was calculated by subtracting 1.30 Å (estimated oxime oxygen atom radius) from the distance of the oxygen atom to the center of the MC ring.

atoms. The Ln^{III} displacement across the series of compounds follows the expected trend for the lanthanide contraction as **11**, which contains Yb^{III}, is only 1.55 Å from the O_{ox}MP. Interestingly, the movement of the trivalent lanthanides by ~0.15 Å closer to the O_{ox}MP across the series of compounds is not reflected by a larger displacement of the sodium ion away from the O_{ox}MP as might have been anticipated on the basis of electrostatic repulsion. Instead, one sees a movement of the Na^I away from the oxime ring caused by the approaching Ln^{III} of only ~0.03 Å. Thus, the Ln^{III}–Na^I separation decreases by ~0.12 Å across the series.

The structures of **1**–**12** are strikingly domed with the Na^I on the underside of the molecule. The Ln^{III} ions are closer to the O_{ox}MP plane, while the Na^I ions are closer to the manganese(III) mean plane (MnMP). Furthermore, the Pr^{III} causes the 12-$MC_{Mn^{III}(N)shi}$-4 framework to be the most domed of the structures. This is evident in the larger average angles (103.95° for **1** to 101.69° for **11**) about the axial coordination of the Mn^{III} ions for **1** (Supporting Information Table S4). Calculation of the centroid produced by the oxime oxygen atoms of the MC ring and then measurement of the angle between the acetate oxygen atom bound to the Mn^{III}, the Mn^{III}, and the centroid, the angle of the Jahn–Teller axis relative to the MC can be determined (Supporting Information Figure S27). This angle can be used as an indication of the planarity of the 12-$MC_{Mn^{III}(N)shi}$-4 framework. Also, the doming of the structure can be inferred from the Ln^{III} ion distance difference between the O_{ox}MP and the MnMP. In **1** the Pr^{III} results in the greatest difference (0.37 Å). This difference decreases upon going from Pr^{III} to Yb^{III} (0.35 Å) indicating that **11** has a less domed structure.

In addition, for compounds **1**–**12** six DMF molecules are located in the lattice, one of which is disordered over two sites. For **1** and **6**, the disorder of a second DMF molecule involves

dx.doi.org/10.1021/ic402865p | Inorg. Chem. 2014, 53, 1729–1742

only the oxygen atom, which is disordered over two alternative sites. For compounds **1**−**11**, which crystallize in the centrosymmetric $P\bar{1}$ space group, there is one independent MC in each unit cell, while for compound **12**, crystallizing in a unit cell metrically the same as in **1**−**11** but in *P*1 with a pseudocenter of inversion but no exact centrosymmetry, there are two independent MCs; thus, for **12** the two MCs are labeled the "A" MC and the "B" MC, and when it is necessary to distinguish the two MCs, the designations **12_A** and **12_B** will be used.

Structural Description of $Na_2(OAc)_2$[12-$MC_{Mn^{III}(N)shi}$-4](DMF)$_6$·2DMF·1.60H_2O. The metallacrown **13** consists of the typical 12-$MC_{Mn^{III}(N)shi}$-4 framework (Figure 5 and

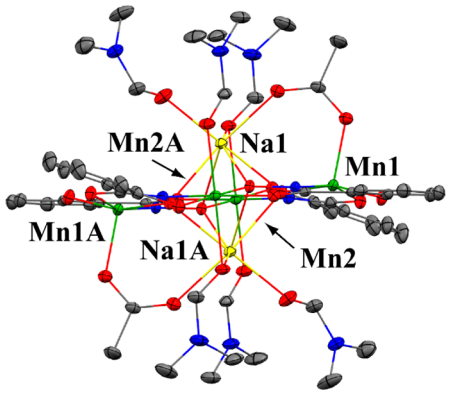

Figure 5. Single-crystal X-ray structure of $Na_2(OAc)_2$[12-$MC_{Mn^{III}(N)shi}$-4](DMF)$_6$·2DMF·1.60H_2O, **13** (side view). The thermal ellipsoid plot of **13** is at 50% probability level. Only the metal atoms are labeled. Hydrogen atoms and the lattice solvent molecules have been omitted for clarity. Color scheme: green, Mn^{III}; yellow, Na^{I}; red, oxygen; blue nitrogen; gray, carbon.

Supporting Information Figure S28). An inversion center is located in the MC central cavity, which generates a Mn−N−O repeat unit that completes an overall square geometry. Two sodium ions are bound on opposite faces of the central cavity. The metallacrown face is nearly planar with two benzene rings slightly bent above and below the plane of the molecule. The greater planarity of **13** is reflected in the smaller average angle between the axial oxygen atom, Mn^{III}, and the centroid of the oxime oxygen atoms (94.65°), and the smaller distance difference (0.01 Å) of the Na^{I} from the O_{ox}MP and the MnMP (Supporting Information Table S4 and Table 3, respectively). Each Mn is assigned an oxidation state of 3+. This is supported by the bond valence sum calculations and average bond distances (Supporting Information Table S1).[24] Furthermore, charge considerations support the oxidation states of the metal ions. The presence of two $^{-}$OAc and four shi^{3-} ligands supports the assignment of four Mn^{III} and two Na^{I}. Mn1 has a coordination number of five with a distorted square pyramidal geometry and an elongated axis approximately perpendicular to the metallacrown plane. The geometry assignment is supported with τ values of 0.01 (Supporting Information Table S2).[25] The basal atoms of the coordination are supplied by the oxime and carbonyl oxygen atoms of one shi^{3-} to form a five-membered chelate ring and on the opposite side oxime nitrogen and phenolate oxygen atoms of a second shi^{3-} form a six-membered chelate ring. The oxygen atom from a bridging acetate anion serves as the apical ligand. The Mn1 to DMF distance of 3.73 Å precludes the description of this atom as a Jahn−Teller distorted, 6-coordinate species. The acetate anions serve to bridge the Mn1 ions to the central Na^{I}. Mn2 has a coordination number of six with distorted octahedral geometry. The equatorial plane atoms of the coordination are supplied by the oxime and carbonyl oxygen atoms of one shi^{3-} to form a five-membered chelate ring and a six-membered chelate ring formed on the opposite side by the oxime nitrogen and phenolate oxygen atoms of a second shi^{3-}. The axial atoms of the elongated Jahn−Teller axis consist of carbonyl oxygen atoms from *trans* DMF molecules. One of the carbonyl oxygen atoms serves as a μ-bridge to the central Na^{I}. The heptacoordinate Na^{I} ion binds to the central cavity of the MC with the four oxime oxygen atoms of the shi^{3-} ligands, and the coordination is completed by a nonbridging carbonyl oxygen atom of a DMF, a carbonyl oxygen atom of a DMF that bridges to Mn2, and an oxygen atom from a bridging acetate anion. The four oxime oxygen atoms form a square base, and the other three oxygen atoms form a triangular face above the face of the metallacrown. In addition, for **13** two partially occupied water molecules and two disordered DMF molecules are located in the lattice. The presence of the water molecule induces disorder in the DMF molecule over two positions.

Unlike the situation with compounds **1**−**12**, **13** has a monovalent ion on the other side of the metallacrown ring from the Na^{I}. As seen in Table 3, the Na^{I} to the O_{ox}MP is only 1.66 Å as compared to complexes **1**−**12**, where this distance was approximately 1.9 Å. The 3.34 Å Na^{I}−Na^{I} separation is 0.12−0.24 Å shorter than the corresponding Ln^{III}−Na^{I} distances observed in **1**−**12**.

Structural Description of $Dy^{III}K(OAc)_4$[12-$MC_{Mn^{III}(N)shi}$-4](DMF)$_4$·DMF. Metallacrown **14** also consists of the typical 12-$MC_{Mn^{III}(N)shi}$-4 framework (Figure 6 and Supporting

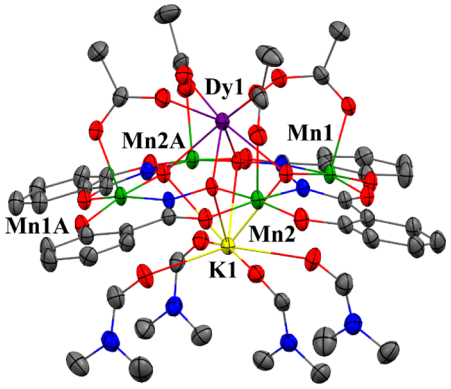

Figure 6. Single-crystal X-ray structure of $Dy^{III}K(OAc)_4$[12-$MC_{Mn^{III}(N)shi}$-4](DMF)$_4$·DMF, **14** (side view). The thermal ellipsoid plot of **14** is at 50% probability level. Only the metal atoms are labeled. Hydrogen atoms and the lattice solvent molecules have been omitted for clarity. Color scheme: purple, Dy^{III}; green, Mn^{III}; yellow, K^{I}; red, oxygen; blue, nitrogen; gray, carbon.

Information Figure S29). A C_2 axis is located in the MC central cavity which generates a Mn−N−O repeat unit that completes an overall square geometry. A lanthanide ion and a potassium ion are bound on opposite faces of the central cavity. The metallacrown is slightly domed with the lanthanide ion captured on the convex side of the central cavity, while a potassium ion is captured on the concave side of the central cavity. The 12-$MC_{Mn^{III}(N)shi}$-4 framework of **14** is domed to a slightly smaller extent compared to **1**−**12**. Compound **14**

dx.doi.org/10.1021/ic402865p | Inorg. Chem. 2014, 53, 1729−1742

possesses a smaller average angle between the axial oxygen atom, Mn^{III}, and the centroid of the oxime oxygen atoms (101.35°) and possesses a smaller distance difference (0.27 Å) of the Ln^{III} from the $O_{ox}MP$ and the MnMP (Supporting Information Table S4 and Table 3, respectively). Each Mn and Ln is assigned an oxidation state of 3+. This is supported by the bond valence sum calculations and average bond distances (Supporting Information Table S1).[24] Furthermore, charge considerations support the oxidation states of the metal ions. The presence of four $^{-}$OAc and four shi^{3-} ligands supports the assignment of four Mn^{III}, one Ln^{III}, and one K^{I}. The coordination numbers and geometries about the Mn^{III} and Dy^{III} ions are strikingly similar to that found for complexes **1**−**12**. Details concerning the τ parameters for the Mn^{III} ions and the skew angles for the Dy^{III} can be found in Supporting Information Tables S2 and S3, respectively. The geometry about the Mn^{III} ions is a distorted square pyramid, and the coordination sphere of Mn^{III} is completed by two shi^{3-} ligands and an apical oxygen atom of a bridging acetate anion. The acetate anions serve to bridge the Mn^{III} ions to the central Dy^{III}. As in **1**−**12**, an alternative description of the polyhedron about the Mn^{III} is that of a highly tetragonally distorted 6-coordinate complex with very long Mn−DMF distances (~2.5 Å). The geometry about the Dy^{III} is best described as a slightly distorted square antiprism, and the coordination sphere of the Dy^{III} is completed by four oxime oxygen atoms and four acetate oxygen atoms. The main structural difference between **14** and **1**−**12** is the coordination of the K^{I} ion. As in **1**−**12**, the octacoordinate K^{I} ion binds to the central cavity of the MC with the oxime oxygen atoms of the shi^{3-} ligands. The difference is that the coordination sphere of the K^{I} is completed by four DMF molecules. As in **1**−**12**, the top four oxime oxygen atoms and bottom four carbonyl oxygen atoms form a severely distorted square antiprism geometry about the K^{I}. The geometry assignment is supported by calculated skew angles (Φ) about the K^{I} that are between both ideal values (Supporting Information Table S3). The potassium ion is further from the $O_{ox}MP$ than observed for the corresponding Dy^{III}/Na^{I} complex, **7**, by 0.31 Å as would be expected due to larger ionic radius of K^{I}. However, comparison of **7** and **14** demonstrates that this relative movement of the potassium ion has no influence on the Dy^{III} distance to the $O_{ox}MP$, which remains 1.59 Å. Accordingly, the Dy^{III}−K^{I} distance increases by only 0.31 Å for **14** when compared to the Dy^{III}−Na^{I} distance of **7**. In addition, for **14** a lattice DMF molecule is disordered over two sites.

DISCUSSION

The preparation of molecular heterometallic species, particularly those that controllably contain three different metals, has been advanced recently.[2] In addition, it is relatively rare that such compounds can be prepared in a one-step high yield synthesis by exploiting molecular self-assembly. We felt that the metallacrown analogy, which has been so effective at forming predictable polymetallic structures of defined composition, would be an excellent entry into such species.

On the basis of this premise, one finds that the $Ln^{III}Na(OAc)_4[12\text{-}MC_{Mn^{III}(N)shi}\text{-}4](H_2O)_4\cdot 6DMF$ compounds, **1**−**12**, can be synthesized in relatively good yield (7−83%) via the simple substitution of the appropriate lanthanide(III) nitrate hydrate salts in the synthetic procedure. This series demonstrates the controllable substitution of the trivalent cation across the series. While we have not examined exhaustively the variability of the alkali metal ion complexation, **14** demonstrates that, at least for the Dy^{III} analogue, **7**, potassium can be easily incorporated at the monovalent cation site. Although we have not examined the variation of either the metallacrown ring inducing ligand salicylhydroximate, shi^{3-}, or the bridging acetates, numerous previous studies have demonstrated that these positions are easily modified through the choice of starting hydroxamic acid or carboxylate salt.[3] Thus, we conclude that hundreds of isostructural hetereotrimetallic derivatives of $Ln^{III}M^{I}L_4[12\text{-}MC_{Mn^{III}(N)L'}\text{-}4]$ are possible by variation with the majority of the lanthanides, at least two alkali metal cations, numerous 12-MC-4 inducing hydroxamates with a 5,6-chelate ring structure, and a broad range of bridging monoanion carboxylates (13 of which are structurally characterized herein). This assessment does not include variation of the Mn^{III} ring metal, which can be substituted to form 12-MC-4 complexes with reported structures containing Fe^{III},[28] Cu^{II},[29] Ni^{II},[30] Zn^{II},[31] $Co^{II/III}$,[32] and Sn^{IV}.[33] Taking this selective modification into account expands the possibilities to over a thousand potential compounds. Thus, this incredibly fertile system potentially allows controllable alternation of five different parameters to vary the physical properties of a single, well-defined structure type.

It should be noted that not all lanthanides yielded structure types **1**−**12**. If La^{III} and Ce^{III} (the largest and lightest of the lanthanides) or Lu^{III} (the smallest and heaviest of the series) were selected as the starting trivalent cations, $Na_2(OAc)_2[12\text{-}MC_{Mn^{III}(N)shi}\text{-}4](DMF)_6$ was recovered. It may be that these three lanthanides, which are at the extremes of size, may not be well adapted for either forming bridges to the Mn^{III} ions or forming strong bonds with the oxime oxygen atoms of the metallacrown ring.

The $Na_2(OAc)_2[12\text{-}MC_{Mn^{III}(N)shi}\text{-}4](DMF)_6$ compound can be made purposely as described in the Experimental Section by the elimination of the appropriate lanthanide nitrate salt, and the structure reported for **13** is for this direct synthesis. The structure of **13** resembles that of other $12\text{-}MC_{Mn^{III}(N)shi}\text{-}4$ compounds that bind two sodium ions: $Na_2Cl_2[12\text{-}MC_{Mn^{III}(N)shi}\text{-}4]DMF_6\cdot 3DMF$, $\mathbf{Na_2Cl_2}$;[7] $Na_2Br_2[12\text{-}MC_{Mn^{III}(N)shi}\text{-}4](DMF)_8$, $\mathbf{Na_2Br_2}$;[6] $Na_2(NCS)_2[12\text{-}MC_{Mn^{III}(N)shi}\text{-}4](DMF)_8$, $\mathbf{Na_2(NCS)_2}$.[8] This new disodium structure contains one bridging acetate that links the cation to the 12-MC-4 as well as the four oxime oxygen atoms. The metrical parameters for **13** (Table 3) are very similar to the metrical parameters for the other three disodium compounds (Supporting Information Table S5). Akin to these other disodium compounds, **13** is nearly planar, forming a stepped structure, as the Na^{I} distance difference between the MnMP and the $O_{ox}MP$ is only 0.01 Å.

The planar orientation of **13** contrasts markedly with that observed for **1**−**12** and **14**. A quick examination of Figure 2b demonstrates that **1** (and all of the compounds containing both a Ln^{III} and an alkali metal ion) is strongly domed, with the alkali cation within the dome and the Ln^{III} and acetates on the exterior face of the structure. A clear visual demonstration of the extent of this doming compared with the disodium complexes is provided by Figure 7, where **1** is shown in green and **13** is represented in red. This comparison is better quantitatively described by examination of the metrical data provided in Table 3 which compares the Ln^{III}−$O_{ox}MP$ distance and the Ln^{III}−MnMP distance. For **1**−**12** the distance difference between these two measurements is significantly greater (0.35 to 0.37 Å for **1**−**12**) than that of the distance

dx.doi.org/10.1021/ic402865p | Inorg. Chem. 2014, 53, 1729−1742

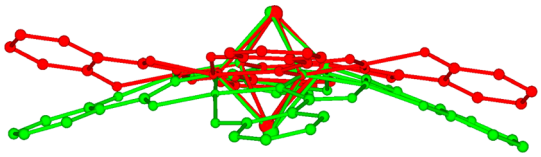

Figure 7. Overlay of the X-ray structures of **1** (green) and **13** (red) with acetates and coordinated solvent molecules removed for clarity. The doming effect of **1** and the stepped structure of **13** are emphasized in this view. The difference of the four atom oxime oxygen planes has been minimized between the two structures for this view.

difference between the Na^{I}–$O_{ox}M$ and Na^{I}–MnMP for **13** (0.01 Å).

The identity of the Ln^{III} influences the structural features of the 12-$MC_{Mn^{III}(N)shi}$-4 framework as listed in Table 3. The largest Ln^{III} investigated was Pr^{III}, **1**. The presence of the larger Pr^{III} leads to an expansion of the 12-$MC_{Mn^{III}(N)shi}$-4 framework. This is clearly evident in the MC cavity radius calculations, average adjacent Mn^{III}–Mn^{III} distances, average cross cavity Mn^{III}–Mn^{III} distances, and average cross cavity oxime oxygen–oxime oxygen distances. Compound **1** has the largest values of all the MCs investigated, while the 12-$MC_{Mn^{III}(N)shi}$-4 framework is the most constrained by the presence of the smallest Ln^{III} ion investigated, Yb^{III} (**11**). Moreover, the values steadily decrease from Pr^{III} to Yb^{III} indicting that the Ln^{III} size consistently affects the 12-$MC_{Mn^{III}(N)shi}$-4 framework. In addition, the distance of the Ln^{III} from the 12-$MC_{Mn^{III}(N)shi}$-4 framework varies based on the identity of the Ln^{III} following the standard lanthanide contraction. The larger Pr^{III} lies farthest from the 12-$MC_{Mn^{III}(N)shi}$-4 framework on the basis of the longer distances from the O_{ox}MP. For compounds **1**–**12** the crystal radius of the Na^{I} does not vary greatly nor does the out of plane displacement from the O_{ox}MP shift significantly (≤0.03 Å). The sodium ion does most closely approach the oxygen ring in **1** and is farthest in **12**. The consequence of the relative invariance of the sodium position is that the smallest Ln^{III} ions have significantly shorter Ln^{III}–Na^{I} separations (Pr^{III}–Na^{I} 3.58 Å vs Yb^{III}–Na^{I} 3.46 Å). Despite the closer distance for Yb^{III}, there is no significant structural perturbation suggesting that the presence of the Na^{I} ion is critical for the molecular doming conformation.

This conclusion is supported by comparing these structures to the corresponding potassium containing complex, **14**, and the previously reported $\{NH(CH_2CH)_3\}_2\{Ca(OBz)_4[12\text{-}MC_{Mn^{III}(N)shi}\text{-}4]\}\cdot 4CH_2Cl_2$, where $^{-}$OBz is benzoate, **Ca(OBz)$_4$**.[10] Comparing the Dy^{III} complexes containing Na^{I} (**7**) and K^{I} (**14**) and despite the fact that the potassium cation of **14** is displaced over 0.3 Å farther from the O_{ox}MP than the sodium cation in **7**, the Dy^{III} ion positions with respect to the same O_{ox}MP are invariant (**7** 1.59 Å vs **14** 1.59 Å). This observation suggests that electrostatic repulsion between ions is negligible. This is not to say that there are no differences in the Dy^{III} position as the Dy^{III}–MnMP distance decreases by nearly a tenth of an angstrom (**7** 1.94 Å vs **14** 1.86 Å) upon potassium substitution. This suggests that the doming of the metallacrown is dependent to some extent on the monovalent cation. Compound **14** appears to be less domed than **7**, as **14** possesses a smaller average angle between the axial oxygen atom, Mn^{III}, and the centroid of the oxime oxygen atoms (**7** 102.40° vs **14** 101.35°) and a smaller distance difference of the Ln^{III} from the O_{ox}MP and the MnMP (**7** 0.35 Å vs **14** 0.27 Å).

This observation raises the question as to whether sodium or potassium is essential for the observed doming. This question may be answered by comparison of **1** with **Ca(OBz)$_4$** as shown in Figure 8 (it should be noted that any of the complexes **2**–**12** and **14** could be substituted for **1** in this analysis). While the top half of **1** and **Ca(OBz)$_4$** are similar in that they contain a cation bound to the metallacrown by four carboxylate oxygen atoms, the calcium complex contains two noncoordinating alkylammonium cations. Examination of Figure 8 demonstrates that both complexes are nearly equivalently domed, despite the absence of Na^{I} or K^{I} in the Ca^{II} structure. This is quantitatively confirmed as shown in Supporting Information Table S6 where the Ca–O_{ox}MP (1.54 Å) and Ca–MnMP (1.80 Å) distances and the difference of these distances (0.26 Å) are consistent with significant doming. Also, the average angle between the axial oxygen atom, Mn^{III}, and the centroid of the oxime oxygen atoms of Ca(OBz)4 is 106.06° (Supporting Information Table S7). For the compounds $Mn(OAc)_2[12\text{-}MC_{Mn^{III}(N)shi}\text{-}4](DMF)_6\cdot 2DMF$, **Mn(OAc)$_2$**,[5] and $Mn(OBz)_2[12\text{-}MC_{Mn^{III}(N)shi}\text{-}4](CH_3OH)_6\cdot 2CH_3OH$, **Mn(OBz)$_2$**,[11] a similar, but smaller, effect can be seen when $Mn^{II}(OAc)_2$ or $Mn^{II}(OBz)_2$ is bound to the 12-MC-4 without a *trans* monovalent cation (Supporting Information Tables S6 and S7). We conclude from these observations that while the monovalent cation may perturb the extent of doming, it is not responsible for the domed conformation.

Given that the monovalent cations *trans* to the lanthanides are not essential for the observed doming of the metallacrown,

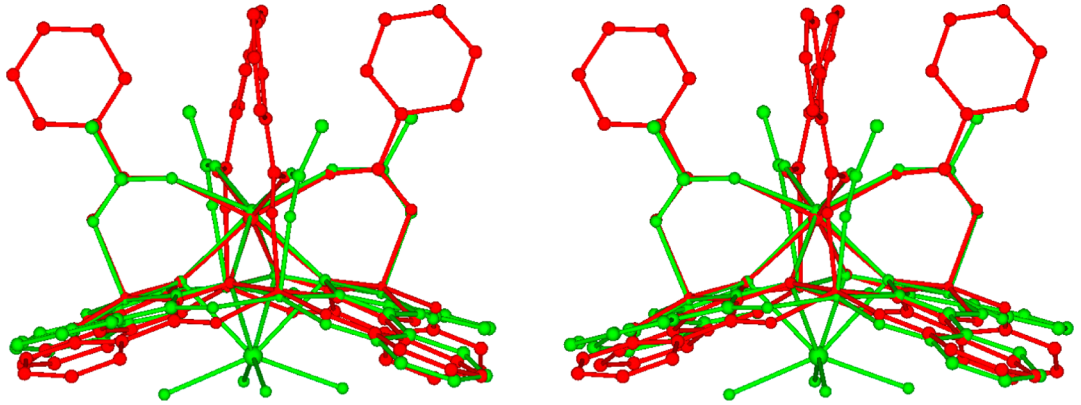

Figure 8. Stereodiagram overlay of the X-ray structures of **1** (green) and **Ca(OBz)$_4$**[10] (red) illustrating the domed structures of both complexes. The difference of the four atom oxime oxygen planes has been minimized between the two structures for this view.

dx.doi.org/10.1021/ic402865p | *Inorg. Chem.* 2014, 53, 1729–1742

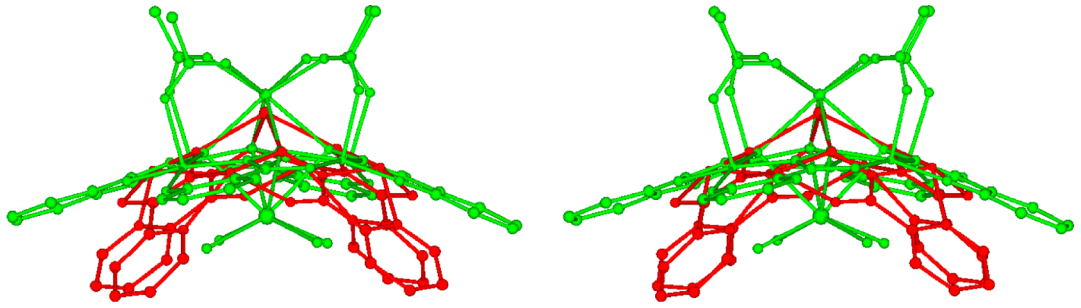

Figure 9. Stereodiagram overlay of the X-ray structures of **6** (green) and **TbZn$_{16}$**[16] (red) illustrating the domed structures of both complexes. The top 12-MC-4 and encircling 24-MC-8 of **TbZn$_{16}$** have been removed for clarity. The difference of the four atom oxime oxygen planes has been minimized between the two structures for this view.

one must consider what other factors might contribute to this conformation. A key consideration is the polyhedron of the metallacrown ring ion, in this case the Mn^{III} ions. A recent analysis of 12-MC-4 structures has appeared when the metallacrown template ligand contained two 5-membered chelate rings rather than the 5,6-fused chelate rings of the salicylhydroximate.[34] In this case, the structures of Ni^{II}[12-$MC_{Ni^{II}(N)picHA}$-4]$^{2+}$ and Zn^{II}[12-$MC_{Zn^{II}(N)picHA}$-4] and the computed structure of Cu^{II}[12-$MC_{Cu^{II}(N)valHA}$-4]$^{2+}$[35] (where H_2picHA= picoline hydroxamic acid and valHA = valine hydroxamic acid) were compared, and it was observed that doming followed the order Zn^{II} > Ni^{II} > Cu^{II} even for cases where the central divalent cation was not displaced from the oxime ring plane. The causative feature was the geometry of the ring metal. In particular, the Zn^{II} had τ values consistent with a square pyramidal complex and was the furthest displaced from the basal ligand mean plane (0.58 Å). What we observe for the [12-$MC_{Mn^{III}(N)shi}$-4] framework is a similar phenomenon with the domed structures containing Mn^{III} that are all displaced out of the plane toward the same face of the metallacrown, which in this case is toward the lanthanide ion. The Mn^{III} ions of **1** are on average displaced from the basal ligand mean plane by 0.17 Å. This is facilitated by the coordinated acetate ligands (or in the case of Ca^{II}, benzoate) that pull the Mn^{III} to that face of the metallacrown.

Recently, the structure of a $Tb^{III}Zn^{II}_{16}$, **TbZn$_{16}$**, complex appeared as a lanthanide sandwich complex formed with two [12-$MC_{Zn^{II}(N)picHA}$-4] species that was encircled by a [24-$MC_{Zn^{II}(N)picHA}$-8].[16] One can approximate the structures of **1**−**12** and **14** by removing the top [12-$MC_{Zn^{II}(N)picHA}$-4] and the [24-$MC_{Zn^{II}(N)picHA}$-8]. A comparison of this molecular fragment, Tb^{III}[12-$MC_{Zn^{II}(N)picHA}$-4], to $Tb^{III}Na(OAc)_4$[12-$MC_{Mn^{III}(N)shi}$-4]$(H_2O)_4$, **6**, reported herein is shown in Figure 9. One sees that, in this case, the greater Zn^{II} displacement from the basal ligand mean plane than the Mn^{III} (average values: Zn^{II} 0.66 Å for $Tb^{III}Zn^{II}_{16}$ vs Mn^{III} 0.17 Å for **6**) leads to greater doming. While it is true that the 5,5-fused chelate rings of the ligand accentuate this effect, it should be remembered that essentially planar Cu^{II}_5 and Ni^{II}_5 type 12-MC-4 structures can be obtained with more in-plane ring metals.[29,30] Once again, a monovalent cation *trans* to the lanthanide is not required for the domed structure. Thus, it appears that the conformation of the ring metal is critical in determining the doming of this class of metallacrowns.

CONCLUSION

The 12 crystal structures of the general formula $Ln^{III}Na(OAc)_4$[12-$MC_{Mn^{III}(N)shi}$-4]$(H_2O)_4$·6DMF complex, where Ln^{III} is Pr^{III} (**1**), Nd^{III} (**2**), Sm^{III} (**3**), Eu^{III} (**4**), Gd^{III} (**5**), Tb^{III} (**6**), Dy^{III} (**7**), Ho^{III} (**8**), Er^{III} (**9**), Tm^{III} (**10**), Yb^{III} (**11**), and Y^{III} (**12**), and $Dy^{III}K(OAc)_4$[12-$MC_{Mn^{III}(N)shi}$-4](DMF)$_4$·DMF (**14**) represent the first heterotrimetallic metallacrowns. The identity of the Ln^{III} influences the 12-$MC_{Mn^{III}(N)shi}$-4 framework as the largest Ln^{III}, Pr^{III}, leads to an expansion of the structure as evident in the largest MC cavity radius and longest average adjacent Mn^{III}−Mn^{III} distances, average cross cavity Mn^{III}−Mn^{III} distances, and average cross cavity oxime oxygen−oxime oxygen distances. In addition, Pr^{III} produces the most domed 12-$MC_{Mn^{III}(N)shi}$-4 framework as evident in the largest average angles about the axial coordination of the ring Mn^{III} ions and the greatest distance difference of the Ln^{III} between the O_{ox}MP and the MnMP. The substitution of K^I for Na^I does not significantly affect the size of the MC cavity, but the K^I ion does affect the planarity of the 12-$MC_{Mn^{III}(N)shi}$-4 framework. For **14**, the 12-$MC_{Mn^{III}(N)shi}$-4 framework is more planar as evident in a smaller average angle about the axial coordination of the ring Mn^{III} ions and a shorter distance difference of the Ln^{III} between the O_{ox}MP and the MnMP.

This new structure type promises a remarkable range of controllable stoichiometries and molecular topologies. On the basis of these studies and previous reports, we can now consider synthesizing compounds of this type with 11 different lanthanides, two different alkali cations, ring metal variants ranging from Mn^{III} to Zn^{II}, a broad range of templating variants of the shi^{3-} ligand, and several different carboxylate bridging groups. Considered together, this suggests thousands of molecular species of controlled topology to which one now has access. By varying each of these parameters one can imagine controllable magnetic interactions to optimize molecular magnetism or develop stable luminescent materials. Future work will investigate the magnetism of **1**−**12**, **14**, and related compounds in particular for single-molecule magnet behavior, as the $Mn^{II}(OAc)_2$[12-$MC_{Mn^{III}(N)shi}$-4] complex showed slow magnetic relaxation. The present class of structures still offers the opportunity for the alignment of magnetoanisotropy vectors within the molecule but now also allows for incorporation of magnetoanisotropy directly from the chosen lanthanide as well as a significant amount of unpaired spin.

ASSOCIATED CONTENT

Supporting Information

X-ray crystallographic information of all structures in CIF format. Additional structural descriptions, crystallographic details, numerical parameters, and figures for each compound. This material is available free of charge via the Internet at http://pubs.acs.org.

dx.doi.org/10.1021/ic402865p | *Inorg. Chem.* 2014, 53, 1729−1742

AUTHOR INFORMATION

Corresponding Authors

*E-mail: vlpec@umich.edu.

*E-mail: cmzaleski@ship.edu.

Present Address

[#]Department of Chemistry and Center of Excellence for Innovation in Chemistry, Faculty of Science, Prince of Songkla University, Hat Yai, Songkhla 90112, Thailand.

Notes

The authors declare no competing financial interest.

ACKNOWLEDGMENTS

C.M.Z., M.R.A., and K.A.Z. acknowledge the Summer Undergraduate Research Experience (SURE) program and the College of Arts & Sciences Faculty-Led Research Fund at Shippensburg University for financial support. V.L.P. thanks the NSF-CHE (Grant 1057331). R.N. acknowledges financial support from the Center of Excellence for Innovation in Chemistry (PERCH-CIC). G.M.F. thanks the NSF-CHE (Grant 1039689) for funding the X-ray diffractometer.

REFERENCES

(1) Doukov, T. I.; Iverson, T. M.; Seravalli, J.; Ragsdale, S. W.; Drennan, C. L. *Science* **2002**, *298*, 567−572.

(2) (a) Berlinguette, C. P.; Dunbar, K. R. *Chem. Commun.* **2005**, 2451−2453. (b) Nesterov, D. S.; Kokozay, V. N.; Dyakonenko, V. V.; Shishkin, O. V.; Jezierska, J.; Ozarowski, A.; Kirillov, A. M.; Kopylovich, M. N.; Pombeiro, A. J. L. *Chem. Commun.* **2006**, 4605−4607. (c) Sutter, J.-P.; Dhers, S.; Costes, J.-P.; Duhayon, C. *C. R. Chim.* **2008**, *11*, 1200−1206. (d) Sutter, J.-P.; Dhers, S.; Rajamani, R.; Ramasesha, S.; Costes, J.-P.; Duhayon, C.; Vendier, L. *Inorg. Chem.* **2009**, *48*, 5820−5828. (e) Dhers, S.; Sahoo, S.; Costes, J.-P.; Duhayon, C.; Ramasesha, S.; Sutter, J.-P. *CrystEngComm* **2009**, *11*, 2078−2083. (f) Long, J.; Chamoreau, L.-M.; Marvaud, V. *Dalton Trans.* **2010**, *39*, 2188−2190. (g) Ladner, L.; Crawford, C.; Assefa, Z.; Sykora, R. E. *Inorg. Chem.* **2011**, *50*, 2199−2206. (h) Nesterov, D. S.; Kokozay, V. N.; Jezierska, J.; Pavlyuk, O. V.; Boča, R.; Pombeiro, A. J. L. *Inorg. Chem.* **2011**, *50*, 4401−4411. (i) Palacios, M. A.; Mota, A. J.; Ruiz, J.; Hänninen, M. M.; Sillanpää, R.; Colacio, E. *Inorg. Chem.* **2012**, *51*, 7010−7012. (j) Li, Z.-Y.; Huang, H.-Q.; Xu, L.; Liu, R.-B.; Zhang, J.-J.; Liu, S.-Q.; Duan, C.-Y. *Cryst. Growth Des.* **2013**, *13*, 918−925.

(3) Mezei, G.; Zaleski, C. M.; Pecoraro, V. L. *Chem. Rev.* **2007**, *107*, 4933−5003.

(4) Tegoni, M.; Furlotti, M.; Tropiano, M.; Lim, C. S.; Pecoraro, V. L. *Inorg. Chem.* **2010**, *49*, 5190−5201.

(5) Lah, M. S.; Pecoraro, V. L. *J. Am. Chem. Soc.* **1989**, *111*, 7258−7259.

(6) Gibney, B. R.; Wang, H.; Kampf, J. W.; Pecoraro, V. L. *Inorg. Chem.* **1996**, *35*, 6184−6193.

(7) Lah, M. S.; Pecoraro, V. L. *Inorg. Chem.* **1991**, *30*, 878−880.

(8) Kessissoglou, D. P.; Bodwin, J. J.; Kampf, J.; Dendrinou-Samara, C.; Pecoraro, V. L. *Inorg. Chim. Acta* **2002**, *331*, 73−80.

(9) Meelich, K.; Zaleski, C. M.; Pecoraro, V. L. *Philos. Trans. R. Soc., B* **2008**, *363*, 1271−1281.

(10) Koumousi, E. S.; Mukherjee, S.; Beavers, C.; Teat, S. J.; Christou, G.; Stamatatos, T. C. *Chem. Commun.* **2011**, *47*, 11128−11130.

(11) Dendrinou-Samara, C.; Papadopoulos, A. N.; Malamatari, D. A.; Tarushi, A.; Raptopoulou, C. P.; Terzis, A.; Samaras, E.; Kessissoglou, D. P. *J. Inorg. Biochem.* **2005**, *99*, 864−875.

(12) Stemmler, A. J.; Kampf, J. W.; Kirk, M. L.; Atasi, B. H.; Pecoraro, V. L. *Inorg. Chem.* **1999**, *38*, 2807−2817.

(13) Cutland, A. D.; Malkani, R. G.; Kampf, J. W.; Pecoraro, V. L. *Angew. Chem., Int. Ed.* **2000**, *39*, 2689−2691.

(14) Cutland, A. D.; Halfen, J. A.; Kampf, J. W.; Pecoraro, V. L. *J. Am. Chem. Soc.* **2001**, *123*, 6211−6212.

(15) Boron, T. T., III; Kampf, J. W.; Pecoraro, V. L. *Inorg. Chem.* **2010**, *49*, 9104−9106.

(16) Jankolovits, J.; Andolina, C. M.; Kampf, J. W.; Raymond, K. N.; Pecoraro, V. L. *Angew Chem. Int. Ed.* **2011**, *50*, 9660−9664.

(17) (a) Piotrowski, H.; Polborn, K.; Hilt, G.; Severin, K. *J. Am. Chem. Soc.* **2001**, *123*, 2699−2700. (b) Piotrowski, H.; Hilt, G.; Schulz, A.; Mayer, P.; Polborn, K.; Severin, K. *Chem.—Eur. J.* **2001**, *7*, 3196−3208. (c) Piotrowski, H.; Severin, K. *Proc. Natl. Acad. Sci. U.S.A.* **2002**, *99*, 4997−5000. (d) Lehaire, M.-L.; Scopelliti, R.; Piotrowski, H.; Severin, K. *Angew. Chem., Int. Ed.* **2002**, *41*, 1419−1422. (e) Grote, Z.; Wizemann, H.-D.; Scopelliti, R.; Severin, K. *Z. Anorg. Allg. Chem.* **2007**, *633*, 858−864. (f) Mezei, G.; Kampf, J. W.; Pan, S.; Poeppelmeier, K. R.; Watkins, B.; Pecoraro, V. L. *Chem. Commun.* **2007**, 1148−1150. (g) Lim, C.-S.; Cutland Van Noord, A.; Kampf, J. W.; Pecoraro, V. L. *Eur. J. Inorg. Chem.* **2007**, 1347−1350. (h) Lim, C.-S.; Kampf, J. W.; Pecoraro, V. L. *Inorg. Chem.* **2009**, *48*, 5224−5233. (i) Rochat, S.; Grote, Z.; Severin, K. *Org. Biomol. Chem.* **2009**, *7*, 1147−1153. (j) Gao, J.; Rochat, S.; Qian, X.; Severin, K. *Chem.—Eur. J.* **2010**, *16*, 5013−5017. (k) Jankolovits, J.; Lim, C.-S.; Mezei, G.; Kampf, J. W.; Pecoraro, V. L. *Inorg. Chem.* **2012**, *51*, 4527−4538. (l) Grant, J. T.; Jankolovits, J.; Pecoraro, V. L. *Inorg. Chem.* **2012**, *51*, 8034−8041. (m) Jankolovits, J.; Cutland-Van Noord, A. D.; Kampf, J. W.; Pecoraro, V. L. *Dalton Trans.* **2013**, *42*, 9803−9808.

(18) (a) Dendrinou-Samara, C.; Alexiou, M.; Zaleski, C. M.; Kampf, J. W.; Kirk, M. L.; Kessissoglou, D. P.; Pecoraro, V. L. *Angew. Chem., Int. Ed.* **2003**, *42*, 3763−3766. (b) Zaleski, C. M.; Depperman, E. C.; Kampf, J. W.; Kirk, M. L.; Pecoraro, V. L. *Angew. Chem., Int. Ed.* **2004**, *43*, 3912−3914. (c) Zaleski, C. M.; Depperman, E. C.; Dendrinou-Samara, C.; Alexiou, M.; Kampf, J. W.; Kessissoglou, D. P.; Kirk, M. L.; Pecoraro, V. L. *J. Am. Chem. Soc.* **2005**, *127*, 12862−12872. (d) Zaleski, C. M.; Depperman, E. C.; Kampf, J. W.; Kirk, M. L.; Pecoraro, V. L. *Inorg. Chem.* **2006**, *45*, 10022−10024. (e) Saalfrank, R. W.; Scheurer, A.; Bernt, I.; Heinemann, F. W.; Postnikov, A. V.; Schünemann, V.; Trautwein, A. X.; Alam, M. S.; Rupp, H.; Müller, P. *Dalton Trans.* **2006**, 2865−2874. (f) Saalrank, R. W.; Scheurer, A.; Prakash, R.; Heinemann, F. W.; Nakajima, T.; Hampel, F.; Leppin, R.; Pilawa, B.; Rupp, H.; Müller, P. *Inorg. Chem.* **2007**, *46*, 1586−1592. (g) Zaleski, C. M.; Kampf, J. W.; Mallah, T.; Kirk, M. L.; Pecoraro, V. L. *Inorg. Chem.* **2007**, *46*, 1954−1956. (h) Wang, S.; Kong, L.; Yang, H.; He, Z.; Jiang, Z.; Li, D.; Zeng, S.; Niu, M.; Dou, J. *Inorg. Chem.* **2011**, *50*, 2705−2707. (i) Zaleski, C. M.; Tricard, S.; Depperman, E. C.; Wernsdorfer, W.; Mallah, T.; Kirk, M. L.; Pecoraro, V. L. *Inorg. Chem.* **2011**, *50*, 11348−11352. (j) Cao, F.; Wang, S.; Li, D.; Zeng, S.; Niu, M.; Song, Y.; Dou, J. *Inorg. Chem.* **2013**, *52*, 10747−10755.

(19) (a) Andruh, M.; Ramade, I.; Codjovi, E.; Guillou, O.; Kahn, O.; Trombe, J. C. *J. Am. Chem. Soc.* **1993**, *115*, 1822−1829. (b) Benelli, C.; Gatteschi, D. *Chem. Rev.* **2002**, *102*, 2369−2387.

(20) (a) Andruh, M.; Costes, J. P.; Diaz, C.; Gao, S. *Inorg. Chem.* **2009**, *48*, 3342−3359. (b) Jeon, I. R.; Clérac, R. *Dalton Trans.* **2012**, *41*, 9569−9586.

(21) (a) Mishra, A.; Wernsdorfer, W.; Abboud, K. A.; Christou, G. *J. Am. Chem. Soc.* **2004**, *126*, 15648−15649. (b) Mereacre, V.; Prodius, D.; Ako, A. M.; Kaur, N.; Lipkowski, J.; Simmons, C.; Dalal, N.; Geru, I.; Anson, C. E.; Powell, A. K.; Turta, C. *Polyhedron* **2008**, *27*, 2459−2463. (c) Akhtar, M. N.; Zheng, Y.-Z.; Lan, Y.; Mereacre, V.; Anson, C. E.; Powell, A. K. *Inorg. Chem.* **2009**, *48*, 3502−3504. (d) Saha, A.; Thomposon, M.; Abboud, K. A.; Wernsdorfer, W.; Christou, G. *Inorg. Chem.* **2011**, *50*, 10476−10485. (e) Papatriantafyllopoulou, C.; Wernsdorfer, W.; Abboud, K. A.; Christou, G. *Inorg. Chem.* **2011**, *50*, 421−423. (f) Chesman, A. S. R.; Turner, D. R.; Berry, K. J.; Chilton, N. F.; Moubaraki, B.; Murray, K. S.; Deacon, G. B.; Batten, S. R. *Dalton Trans.* **2012**, *41*, 11402−11412. (g) Ke, H.; Zhao, L.; Guo, Y.; Tang, J. *Dalton Trans.* **2012**, *41*, 2314−2319. (h) Chen, H.; Ma, C.-B.; Hu, M.-Q.; Wen, H.-M.; Cui, H.-H.; Liu, J.-Y.; Song, X.-W.; Chen, C.-N. *Dalton Trans.* **2013**, *42*, 4908−4914. (i) Guedes, G. P.; Soriano, S.; Mercante, L. A.; Speziali, N. L.; Novak, M. A.; Andruh, M.; Vaz, M. G. F. *Inorg. Chem.* **2013**, *52*, 8309−8311. (j) Alexandropoulos, D. I.; Nguyen, T. N.; Cunha-Silva, L.; Zafiropoulos, T. F.; Escuer, A.; Christou, G.; Stamatatos, T. C. *Inorg. Chem.* **2013**, *52*, 1179−1181.

(k) Chandrasekhar, V.; Bag, P.; Speldrich, M.; van Leusen, J.; Kögerler, P. *Inorg. Chem.* **2013**, *52*, 5035−5044.
(22) Zaleski, C. M.; Lim, C.-S.; Cutland-Van Noord, A. D.; Kampf, J. W.; Pecoraro, V. L. *Inorg. Chem.* **2011**, *50*, 7707−7717.
(23) Shannon, R. D. *Acta Crystallogr.* **1976**, *A32*, 751−767.
(24) (a) Liu, W.; Thorp, H. H. *Inorg. Chem.* **1993**, *32*, 4102−4105. (b) Trzesowska, A.; Kruszynski, R.; Bartczak, T. J. *Acta Crystallogr.* **2004**, *B60*, 174−178. (c) Krivovichev, S. V. *Z. Kristallogr.* **2012**, *227*, 575−579.
(25) Addison, A. W.; Rao, T. N.; Reedijk, J.; van Rijn, J.; Verschoor, G. G. *J. Chem. Soc., Dalton Trans.* **1984**, *7*, 1349−1356.
(26) (a) AlDamen, M. A.; Clemente-Juan, J. M.; Coronado, E.; Martí-Gastaldo, C.; Gaita-Ariño, A. *J. Am. Chem. Soc.* **2008**, *130*, 8874−8875. (b) AlDamen, M. A.; Cardona-Serra, S.; Clemente-Juan, J. M.; Coronado, E.; Gaita-Ariño, A.; Martí-Gastaldo, C.; Luis, F.; Montero, O. *Inorg. Chem.* **2009**, *48*, 3467−3479.
(27) Macrae, C. F.; Edgington, P. R.; McCabe, P.; Pidcock, E.; Shields, G. P.; Taylor, R.; Towler, M.; van de Streek, J. *J. Appl. Crystallogr.* **2006**, *39*, 453−457.
(28) Lah, M. S.; Pecoraro, V. L. *Comments Inorg. Chem.* **1990**, *11*, 59−84.
(29) (a) Kurzak, B.; Farkas, E.; Glowiak, T.; Kozlowski, H. *J. Chem. Soc., Dalton Trans.* **1991**, 163−167. (b) Orama, M.; Saarinen, H.; Korvenranta, J.; Raikas, T. *Acta Chem. Scand.* **1992**, *46*, 1083−1086. (c) Orama, M.; Saarinen, H.; Korvenranta, J. *Acta Chem. Scand.* **1994**, *48*, 127−133. (d) Gibney, B. R.; Kessissoglou, D. P.; Kampf, J. W.; Pecoraro, V. L. *Inorg. Chem.* **1994**, *33*, 4840−4849. (e) Halfen, J. A.; Bodwin, J. J.; Pecoraro, V. L. *Inorg. Chem.* **1998**, *37*, 5416−5417. (f) Bodwin, J. J.; Pecoraro, V. L. *Inorg. Chem.* **2000**, *39*, 3434−3435. (g) Song, Y.; Liu, J.-C.; Liu, Y.-J.; Zhu, D.-R.; Zhuang, J.-Z.; You, X.-Z. *Inorg. Chim. Acta* **2000**, *305*, 135−142. (h) Gaynor, D.; Starikova, Z. A.; Haase, W.; Nolan, K. B. *J. Chem. Soc., Dalton Trans.* **2001**, 1578−1581. (i) Tegoni, M.; Ferretti, L.; Sansone, F.; Remelli, M.; Bertolasi, V.; Dallavalle, F. *Chem.—Eur. J.* **2007**, *13*, 1300−1308. (j) Gumienna-Kontecka, E.; Golenya, I. A.; Dudarenko, N. M.; Dobosz, A.; Haukka, M.; Fritsky, I. O.; Swiatek-Kozlowska, J. *New J. Chem.* **2007**, *31*, 1798−1805. (k) Pavilshchuk, A. V.; Kolotilov, S. V.; Zeller, M.; Shvets, O. V.; Fritsky, I. O.; Lofland, S. E.; Addison, A. W.; Hunter, A. D. *Eur. J. Inorg. Chem.* **2011**, 4826−4836. (l) Lago, A. B.; Pasán, J.; Cañadillas-Delgado, L.; Fabelo, O.; Casado, F. J. M.; Julve, M.; Lloret, F.; Ruiz-Pérez, C. *New J. Chem.* **2011**, *35*, 1817−1822. (m) Herring, J.; Zeller, M.; Zaleski, C. M. *Acta Crystallogr.* **2011**, *E67*, m419−m420. (n) McDonald, C.; Whyte, T.; Taylor, S. M.; Sanz, S.; Brechin, E. K.; Gaynor, D.; Jones, L. F. *CrystEngComm* **2013**, *15*, 6672−6681.
(30) (a) Stemmler, A. J. *Synthetic Strategies for Expanding the Scope of Metallacrowns*. Ph.D. Dissertation, University of Michigan, Ann Arbor, MI, 1996. (b) Psomas, G.; Stemmler, A. J.; Dendrinou-Samara, C.; Bodwin, J. J.; Scheider, M.; Alexiou, M.; Kampf, J. W.; Kessissoglou, D. P.; Pecoraro, V. L. *Inorg. Chem.* **2001**, *40*, 1562−1570. (c) Alexiou, M.; Tsivikas, I.; Dendrinou-Samara, C.; Pantazaki, A. A.; Trikalitis, P.; Lalioti, N.; Kyriakidis, D. A.; Kessissoglou, D. P. *J. Inorg. Biochem.* **2003**, *93*, 256−264. (d) Psomas, G.; Dendrinou-Samara, C.; Alexiou, M.; Tsohos, A.; Raptopoulou, C. P.; Terzis, A.; Kessissoglou, D. P. *Inorg. Chem.* **1998**, *37*, 6556−6557. (e) Tsivikas, I.; Alexiou, M.; Pantazaki, A. A.; Dendrinou-Samara, C.; Kyriakidis, D. A.; Kessissoglou, D. P. *Bioinorg. Chem. Appl.* **2003**, *1*, 85−97. (f) Denrinou-Samara, C.; Psomas, G.; Iordanidis, L.; Tangoulis, V.; Kessissoglou, D. P. *Chem.—Eur. J.* **2001**, *7*, 5041−5051. (g) Mandal, D.; Bertolasi, V.; Aromí, G.; Ray, D. *Dalton Trans.* **2007**, 1989−1992. (h) Audhya, A.; Maity, M.; Bhattacharya, K.; Clérac, R.; Chaudhury, M. *Inorg. Chem.* **2010**, *49*, 9026−9035.
(31) (a) Stemmler, A. J.; Kampf, J. W.; Pecoraro, V. L. *Inorg. Chem.* **1995**, *34*, 2271−2272. (b) Alexiou, M.; Dendrinou-Samara, C.; Raptopoulou, C. P.; Terzis, A.; Kessissoglou, D. P. *Inorg. Chem.* **2002**, *41*, 4732−4738. (c) Song, J.-L.; Mao, J.-G.; Zeng, H.-Y.; Kremer, R. K.; Dong, Z.-C. *Inorg. Chem. Commun.* **2003**, *6*, 891−895. (d) Alexiou, M.; Katsoulakou, E.; Dendrinou-Samara, C.; Raptopoulou, C. P.; Psycharis, V.; Manessi-Zoupa, E.; Perlepes, S. P.; Kessissoglou, D. P. *Eur. J. Inorg. Chem.* **2005**, 1964−1978. (e) Konidaris, K. F.; Bekiari, V.; Katsoulakou, E.; Raptopoulou, C. P.; Psycharis, V.; Manessi-Zoupa, E.; Kostakis, G. E.; Perlepes, S. P. *Dalton Trans.* **2012**, *41*, 3797−3806.
(32) (a) Stamatatos, T. C.; Dionyssopoulou, S.; Efthymiou, G.; Kyritsis, P.; Raptopoulou, C. P.; Terzis, A.; Vicente, R.; Escuer, A.; Perlepes, S. P. *Inorg. Chem.* **2005**, *44*, 3374−3376. (b) Stamatatos, T. C.; Papatriantafyllopoulou, C.; Katsoulakou, E.; Raptopaolou, C. P.; Perlepes, S. P. *Polyhedron* **2007**, *26*, 1830−1834.
(33) (a) Zhao, X.-J.; Li, D.-C.; Zhang, Q.-F.; Wang, D.-Q.; Dou, J.-M. *Inorg. Chem. Commun.* **2010**, *13*, 346−349. (b) Zhao, X.-J.; Zhang, Q.-F.; Li, D.-C.; Dou, J.-M.; Wang, D.-Q. *J. Organomet. Chem.* **2010**, *695*, 2134−2141.
(34) Jankolovits, J.; Kampf, J. W.; Pecoraro, V. L. *Inorg. Chem.* **2013**, *52*, 5063−5076.
(35) Tegoni, M.; Remelli, M.; Bacco, D.; Marchiò, L.; Dallavalle, F. *Dalton Trans.* **2008**, 2693−2701.